4. EXPLANATORY NOTES[1]

Shipboard Scientific Party[2]

INTRODUCTION

In this chapter, we have assembled information that will help the reader understand the basis for our preliminary conclusions and also help the interested investigator select samples for further analysis. This information concerns only shipboard operations and analyses described in the site reports in the *Initial Reports* volume of the Leg 131 *Proceedings of the Ocean Drilling Program*. Methods used by various investigators for shore-based analysis of Leg 131 data will be detailed in the individual scientific contributions published in the *Scientific Results* volume.

AUTHORSHIP OF SITE CHAPTER

The separate sections of the site chapter were written by the following shipboard scientists (authors are listed in alphabetical order, no seniority is necessarily implied):

Principal Results (Hill, Taira)
Background and Objectives (Hill, Taira)
Operations (Firth, Foss, Pettigrew)
Lithostratigraphy (Pickering, Underwood)
Biostratigraphy (Firth, Kato, Olafsson)
Structural Geology (Byrne, Karig, Lallemant, Maltman)
Paleomagnetics (Lu, Owens)
Inorganic Geochemistry (Gamo, Gieskes, Kastner)
Organic Geochemistry (Berner)
Basement Lithology and Geochemistry (Siena)
Physical Properties (Bruckmann, Moran, Taylor, Zhang)
Anelastic Strain Recovery (Karig)
Downhole Measurements (Fisher, Hyndman, Moore)
Packer Experiments (Fisher)
LAST (Moran)
ONDO (Yamano)
Seismic Stratigraphy and VSP (Moore)
Heat Flow (Fisher, Foucher, Hyndman, Yamano)
Sediment Accumulation Rates (Firth, Olafsson, Owens, Taylor)
Clay Instability Tests (Wilkinson)
Appendixes: Shipboard Scientific Party

Summary core descriptions ("barrel sheets" and igneous rock visual core descriptions) and photographs of each core appear at the end of the volume.

Use of Ma vs m.y.

1. Ma is equivalent to and replaces m.y.B.P. (million years Before Present), e.g., 35–40 Ma.
2. m.y. is used in sentences such as, " . . . for 5 m.y. in the early Miocene."

DRILLING CHARACTERISTICS

Information concerning sedimentary stratification in uncored or unrecovered intervals may be inferred from seismic data, wireline-logging results, and from an examination of the behavior of the drill string as observed and recorded on the drilling platform. Typically, the harder a layer, the slower and more difficult it is to penetrate. A number of other factors may determine the rate of penetration, so it is not always possible to relate the drilling time directly to the hardness of the layers. Bit weight and revolutions per minute, recorded on the drilling recorder, also influence the penetration rate.

DRILLING DEFORMATION

When cores are split, many show signs of significant sediment disturbance, including the concave-downward appearance of originally horizontal bands, haphazard mixing of lumps of different lithologies (mainly at the tops of cores), and the near-fluid state of some sediments recovered from tens to hundreds of meters below the seafloor. Core deformation probably occurs during cutting, retrieval (with accompanying changes in pressure and temperature), and core handling on deck. A detailed discussion of slump-like drilling disturbance is given in the "Core Description" section of this chapter.

SHIPBOARD SCIENTIFIC PROCEDURES

Numbering of Sites, Holes, Cores, and Samples

ODP drill sites are numbered consecutively, and refer to one or more holes drilled while the ship was positioned over one acoustic beacon. Multiple holes may be drilled at a single site by pulling the drill pipe above the seafloor (out of the hole), moving the ship some distance from the previous hole, and then drilling another hole.

For all ODP drill sites, a letter suffix distinguishes each hole drilled at the same site. For example, the first hole drilled is assigned the site number modified by the suffix A, the second hole takes the site number and suffix B, and so forth. Note that this procedure differs slightly from that used by DSDP (Sites 1 through 624), but prevents ambiguity between site- and hole-number designations. It is important to distinguish among holes drilled at a site, because recovered sediments or rocks from different holes usually do not come from equivalent positions in the stratigraphic column.

The cored interval is measured in meters below seafloor (mbsf). The depth interval assigned to an individual core begins with the depth below the seafloor where the coring operation began, and extends to the depth that the coring operation ended (see Fig. 1). For example, each coring interval is generally up to 9.5 m long, which is the length of a core barrel. Coring intervals may be shorter and may not necessarily be adjacent if separated by drilled intervals. In soft sediments, the drill string can be "washed ahead" with the core barrel in place, without recovering sediments. This is achieved by pumping water down the pipe at high pressure to wash the sediment out of the way of the bit and up the annulus

[1] Taira, A., Hill, I., Firth, J., et al., 1991. *Proc. ODP, Init. Repts.*, 131: College Station, TX (Ocean Drilling Program).
[2] Shipboard Scientific Party is as given in the list of participants preceding the contents.

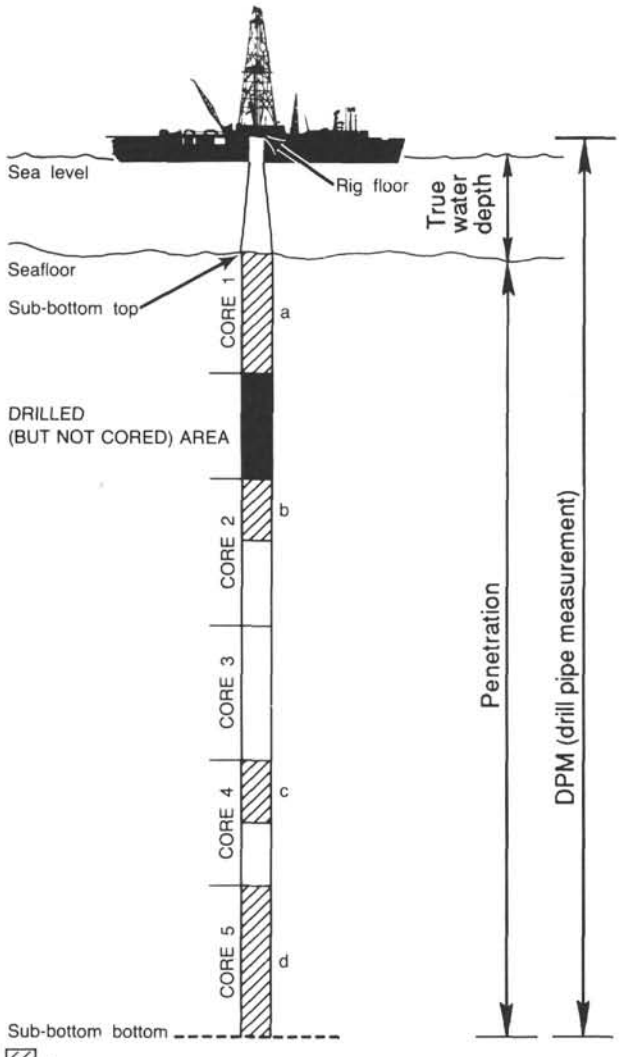

BOTTOM FELT: *distance from rig floor to seafloor*

TOTAL DEPTH: distance from rig floor to bottom of hole (sub-bottom bottom)

PENETRATION: distance from seafloor to bottom of hole (sub-bottom bottom)

NUMBER OF CORES: total of all cores recorded, including cores with no recovery

TOTAL LENGTH OF CORED SECTION: distance from sub-bottom top to sub-bottom bottom minus drilled (but not cored) areas in between

TOTAL CORE RECOVERED: total from adding a, b, c, and d *in diagram*

CORE RECOVERY (%): equals TOTAL CORE RECOVERED divided by TOTAL LENGTH OF CORED SECTION times 100

Figure 1. Diagram of terms used to discuss coring operations and core recovery.

between the drill pipe and the wall of the hole. If thin, hard, rock layers are present, then it is possible to get "spotty" sampling of these resistant layers within the washed interval, and thus to have a cored interval greater than 9.5 m. In drilling hard rock, a center bit may replace the core barrel if it is necessary to drill without core recovery.

Cores taken from a hole are numbered serially from the top of the hole downward. Core numbers and their associated cored intervals in meters below seafloor usually are unique in a given hole; however, this may not be true if an interval must be cored twice, because of caving of cuttings or other hole problems. Maximum full recovery for a single core is 9.5 m of rock or sediment contained in a plastic liner (6.6 cm internal diameter) plus about 0.2 m (without a plastic liner) in the core catcher (Fig. 2). The core catcher is a device at the bottom of the core barrel that prevents the core from sliding out when the barrel is being retrieved from the hole. In certain situations (e.g., when coring gas-charged sediments that expand while being brought on deck), recovery may exceed the 9.5-m maximum.

A recovered core is divided into 1.5-m sections that are numbered serially from the top (Fig. 2). When full recovery is obtained, the sections are numbered from 1 through 7, with the last section possibly being shorter than 1.5 m (rarely, an unusually long core may require more than seven sections). When less than full recovery is obtained, there will be as many sections as needed to accommodate the length of the core recovered; for example, 4 m of core would be divided into two 1.5-m sections and one 1-m section. If cores are fragmented (recovery less than 100%), sections are numbered serially and

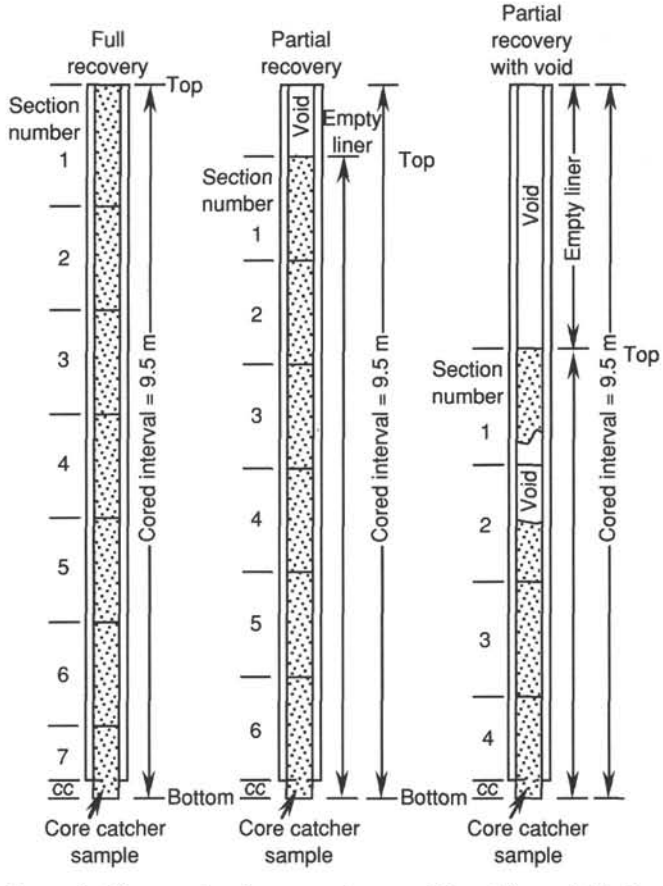

Figure 2. Diagram showing procedure used in cutting and labeling recovered core sections.

intervening sections are noted as void, whether shipboard scientists believe that the fragments were contiguous *in-situ* or not. In rare cases a section less than 1.5 m may be cut to preserve features of interest (e.g., lithological contacts).

By convention, material recovered from the core catcher is placed below the last section when the core is described, and labeled core catcher (CC); in sedimentary cores, it is treated as a separate section. The core catcher is placed at the top of the cored interval in cases where material is only recovered in the core catcher. However, information supplied by the drillers or by other sources may allow for more precise interpretation as to the correct position of core-catcher material within an incompletely recovered cored interval.

Igneous rock cores are also cut into 1.5-m sections that are numbered serially; each piece of rock is then assigned a number. Fragments of a single piece are assigned a single number, and individual fragments are identified alphabetically. The core-catcher sample is placed at the bottom of the last section and is treated as part of the last section, rather than separately. Scientists completing visual core descriptions describe each lithologic unit, noting core and section boundaries only as physical reference points.

When, as is usually the case, the recovered core is shorter than the cored interval, the top of the core is equated with the top of the cored interval by convention, to achieve consistency in handling analytical data derived from the cores. Samples removed from the cores are designated by distance measured in centimeters from the top of the section to the top and bottom of each sample removed from that section. In curated hard rock sections, sturdy plastic spacers are placed between pieces that did not fit together to protect them from damage in transit and in storage; therefore, the centimeter interval noted for a hard rock sample has no direct relationship to that sample's depth within the cored interval, but is only a physical reference to the location of the sample within the curated core.

A full identification number for a sample consists of the following information: leg, site, hole, core number, core type, section number, piece number (for hard rock), and interval in centimeters measured from the top of section. For example, a sample identification "131-808A-5H-1, 10–12 cm" would be interpreted as representing a sample removed from the interval between 10 and 12 cm below the top of Section 1, Core 5 (H indicates that this core was taken during hydraulic piston coring) of Hole 808A during Leg 131.

All ODP core and sample identifiers indicate core type. The following abbreviations are used: R = Rotary Core Barrel (RCB); H = Hydraulic Piston Core (HPC; also referred to as APC, or Advanced Hydraulic Piston Core); P = Pressure Core Sampler; X = Extended Core Barrel (XCB); B = drill-bit recovery; C = center-bit recovery; I = *in-situ* water sample; S = sidewall sample; W = wash-core recovery; and M = miscellaneous material. APC, XCB, RCB, P, and W cores were cut on Leg 131.

Core Handling

Sediments

As soon as a core is retrieved on deck, a sample is taken from the core catcher and given to the paleontological laboratory for an initial age assessment. The core is then placed on the long horizontal rack, and gas samples may be taken by piercing the core liner and withdrawing gas into a vacuum-tube. Voids within the core are sought as sites for gas sampling. Some of the gas samples are stored for shore-based study, but others are analyzed immediately as part of the shipboard safety and pollution-prevention program. Next, the core is marked into section lengths, each section is labeled, and the core is cut into sections. Interstitial-water (IW) and organic geochemistry (OG) samples are then taken. In addition, some headspace gas samples are scraped from the ends of cut sections on the catwalk, and sealed in glass vials for light hydrocarbon analysis. Each section is then sealed at the top and bottom by gluing on color-coded plastic caps, blue to identify the top of a section and clear for the bottom. A yellow cap is placed on the section ends from which a whole-round sample has been removed, and the sample code (e.g., IW) is written on the yellow cap. The caps are usually attached to the liner by coating the end liner and the inside rim of the cap with acetone, and then the caps are taped to the liners.

The cores then are carried into the laboratory, where the sections are again labeled, using an engraver to permanently mark the full designation of the section. The length of the core in each section and the core-catcher sample are measured to the nearest centimeter; this information is logged into the shipboard CORELOG database program.

Whole-round sections from APC and XCB cores are normally run through the multisensor track (MST). The MST includes the GRAPE (gamma-ray attenuation porosity evaluator) and *P*-wave logger devices, which measure bulk density, porosity, and sonic velocity, and also includes a meter that determines the volume magnetic susceptibility. At this point, whole-round samples for physical properties (PP) and structural analysis are taken. In well lithified sedimentary cores, the core liner is split and the top half removed so that the whole-round core can be observed before choosing the samples. Relatively soft sedimentary cores are equilibrated to room temperature (approximately 3 hr), and thermal conductivity measurements are performed on them.

Cores of soft material are split lengthwise into working and archive halves. The softer cores are split with a wire or saw, depending on the degree of induration. Harder cores are split with a band saw or diamond saw. The wire-cut cores are split from the bottom to top, so investigators should be aware that older material could have been transported up the core on the split face of each section.

The working half of the core is sampled for both shipboard and shore-based laboratory studies. Each extracted sample is logged into the sampling computer database program by the location and the name of the investigator receiving the sample. Records of all removed samples are kept by the curator at ODP. The extracted samples are sealed in plastic vials or bags and labeled. Samples are routinely taken for shipboard physical property analysis. These samples are subsequently used for calcium carbonate (coulometric analysis), organic carbon (CNS elemental analyzer), and X-ray diffraction (XRD) analysis, and the data are reported in the site chapter.

The archive half is described visually. Smear slides are made from samples taken from the archive half and are supplemented by thin sections taken from the working half. Most archive sections are run through the cryogenic magnetometer. The archive half is then photographed with both black-and-white and color film, a whole core at a time. Close-up photographs (black-and-white) are taken of particular features for illustrations in the summary of each site, as requested by individual scientists.

Both halves of the core are then put into labeled plastic tubes, sealed, and transferred to cold-storage space aboard the drilling vessel. At the end of the leg, the cores are transferred from the ship in refrigerated airfreight containers to cold storage at the Gulf Coast Repository at the Ocean Drilling Program, Texas A&M University, College Station, Texas.

Igneous and Metamorphic Rocks

Igneous and metamorphic rock cores are handled differently from sedimentary cores. Once on deck, the core-catcher is placed at the bottom of the core liner and total core recovery is calculated by shunting the rock pieces together and measuring to the nearest centimeter; this information is logged into the shipboard core-log database program. The core is then cut into 1.5-m-long sections and transferred into the lab.

The contents of each section are transferred into 1.5-m-long sections of split core liner, where the bottom of oriented pieces (i.e., pieces that clearly could not have rotated top to bottom about a horizontal axis in the liner) are marked with a red wax pencil. This is to ensure that orientation is not lost during the splitting and labeling process. The core is then split into archive and working halves. A plastic spacer is used to separate individual pieces and/or reconstructed groups of pieces in the core liner. These spacers may represent a substantial interval of no recovery. Each piece is numbered sequentially from the top of each section, beginning with number 1; reconstructed groups of pieces are assigned the same number, but are lettered consecutively. Pieces are labeled only on external surfaces. If the piece is oriented, an arrow is added to the label pointing to the top of the section.

The working half of the hard-rock core is then sampled for shipboard laboratory studies. Records of all samples are kept by the curator at ODP. Minicore samples are routinely taken for physical properties and magnetic studies. Some of these samples are later subdivided for XRF analysis and thin-sectioning, so that as many measurements as possible are made on the same pieces of rock. At least one minicore is taken per lithological unit when recovery permits, generally from the freshest areas of core. Additional thin sections, X-ray diffraction (XRD) samples, and X-ray fluorescence (XRF) samples are selected from areas of particular interest. Samples for shore-based studies are selected in a sampling party held after drilling has ended.

The archive half is described visually, then photographed with both black-and-white and color film, one core at a time. Both halves of the core are then shrink-wrapped in plastic to prevent rock pieces from vibrating out of sequence during transit, put into labeled plastic tubes, sealed, and transferred to cold-storage space aboard the drilling vessel.

VISUAL CORE DESCRIPTIONS

Sediment "Barrel Sheets"

The core-description forms (Fig. 3), or "barrel sheets," summarize the data obtained during shipboard analysis of each sediment core. The following discussion explains the ODP conventions used in compiling each part of the core-description forms and the exceptions to these procedures adopted by the Shipboard Scientific Party.

Shipboard sedimentologists were responsible for visual core logging, smear-slide analyses, and thin-section descriptions of sedimentary and volcaniclastic material. Mineral-composition data were determined by X-ray diffraction, and these data augment the visual core descriptions. Data on biostratigraphy (age), geochemistry ($CaCO_3$, C_{org}), magnetics, and physical properties (wet-bulk density and porosity) also were integrated with the sedimentologic information.

Core Designation

Core designations specify the leg, site, hole, core number, and core type, as discussed in a preceding section (see "Numbering of Sites, Holes, Cores, and Samples" section, this chapter). The cored interval is specified in terms of meters below sea level (mbsl) and meters below seafloor (mbsf). On the basis of drill-pipe measurements (dpm), which are reported by the SEDCO coring technician and the ODP operations superintendent, depths are corrected for the height of the rig floor dual elevator stool above sea level to give true water depth and correct mbsl.

Paleontological Data

Microfossil abundances, preservation, and zone assignments appear on the core-description form under the heading "Biostrat. Zone/Fossil Character." The chronostratigraphic unit, as defined by paleontological results, is shown in the "Time-Rock Unit" column. Detailed information on the zonations, together with terms used to report abundance and preservation, are presented in the "Biostratigraphy" section (this chapter).

Paleomagnetic, Physical Property, and Chemical Data

Columns on the core-description form display the results of paleomagnetic measurements (normal, reversed, or unknown polarity, shown as "N", "R", or "?", respectively), physical property values (wet-bulk density and porosity), and chemical data (percentages of $CaCO_3$ determined with the Coulometrics analyzer). Additional information on shipboard procedures for collecting these types of data appears in the "Paleomagnetism," "Physical Properties," and "Organic Geochemistry" sections (this chapter).

Graphic Lithology Column

The lithologies of the material recovered are illustrated graphically on the core description forms, either by a single pattern or by two or more patterns (see Fig. 4). Where an interval of sediment or sedimentary rock is a mixture of different lithologies, the constituent categories are separated by a solid vertical line, and each lithology is represented by its own pattern. Constituents that comprise less than 25% of the sediment are not put in the graphic lithology column but, instead, are listed in the "Lithologic Description" section of the barrel sheet. Where an interval is composed of thin layers of two or more interbedded sediment types that have quite different characteristics, the average relative abundances of the constituents are represented graphically by dashed lines that vertically divide the interval into appropriate fractions as described above.

Only intervals exceeding 10 cm can be displayed in the graphic lithology column at the scale provided. Information on finer-scale lithologic variations is included in the VCD (Visual Core Description) forms available from ODP upon request. Where sedimentary material is intercalated with igneous rocks, the character of the igneous section is recorded under "Hard Rock Core Description Forms." These intervals are labeled on the sedimentary barrel sheets as "see igneous rock description."

Sedimentary Structures

In sediment cores, some natural structures can be difficult to distinguish from structures created by the coring process. Natural structures are illustrated by symbols in the "Sedimentary Structure" column of the core-description form. Figure 5 shows all of the symbols used during Leg 131 to describe the primary biogenic and physical sedimentary structures. The most common types of structures include scoured basal contacts, graded beds, cross lamination, parallel laminae, and various degrees of bioturbation. The classification scheme for structures caused by tectonic deformation of the sediments

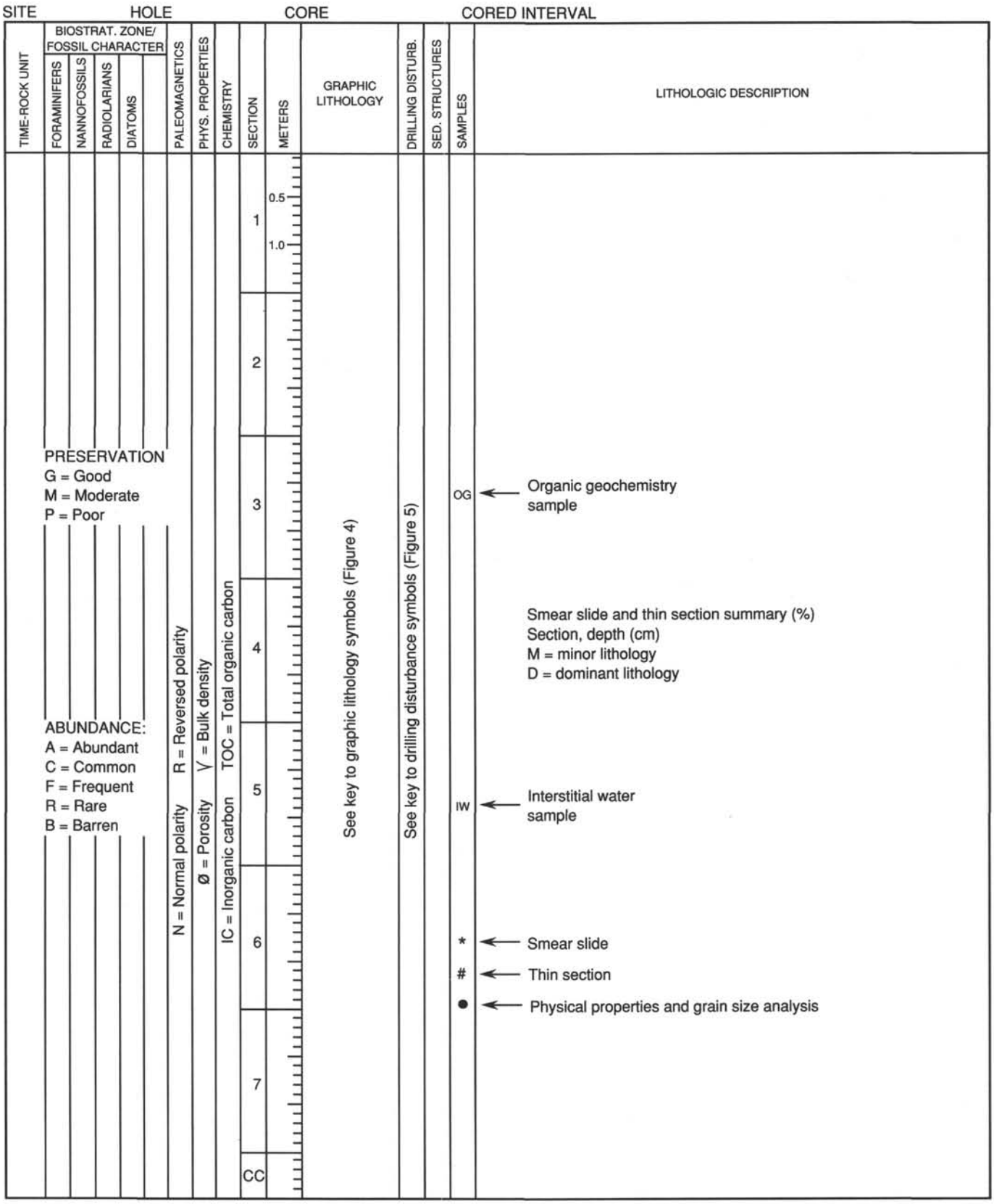

Figure 3. Core description form ("barrel sheet") used for sediments and sedimentary rocks.

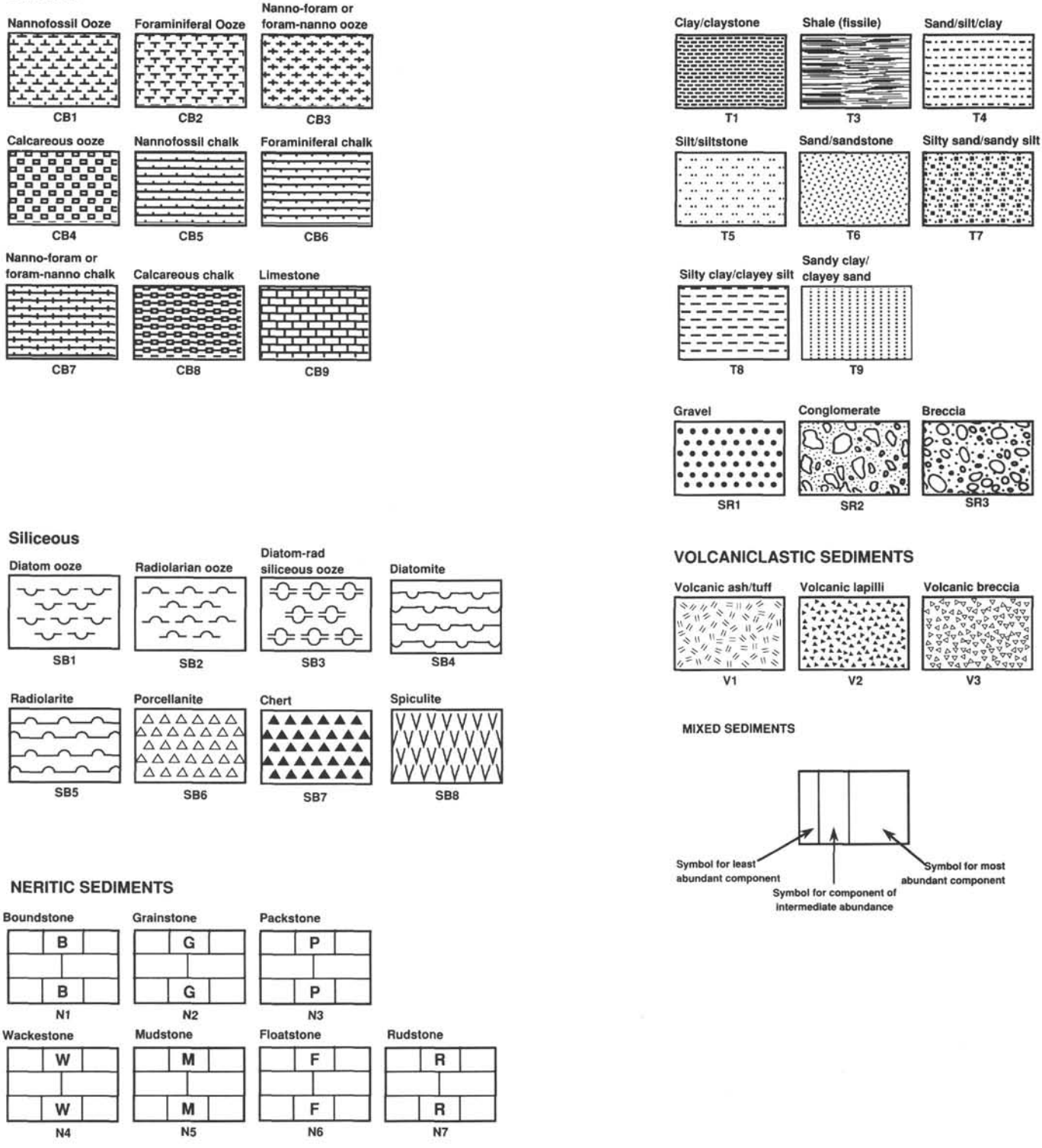

Figure 4. Key to symbols used in the "graphic lithology" column on the core description form shown in Figure 3.

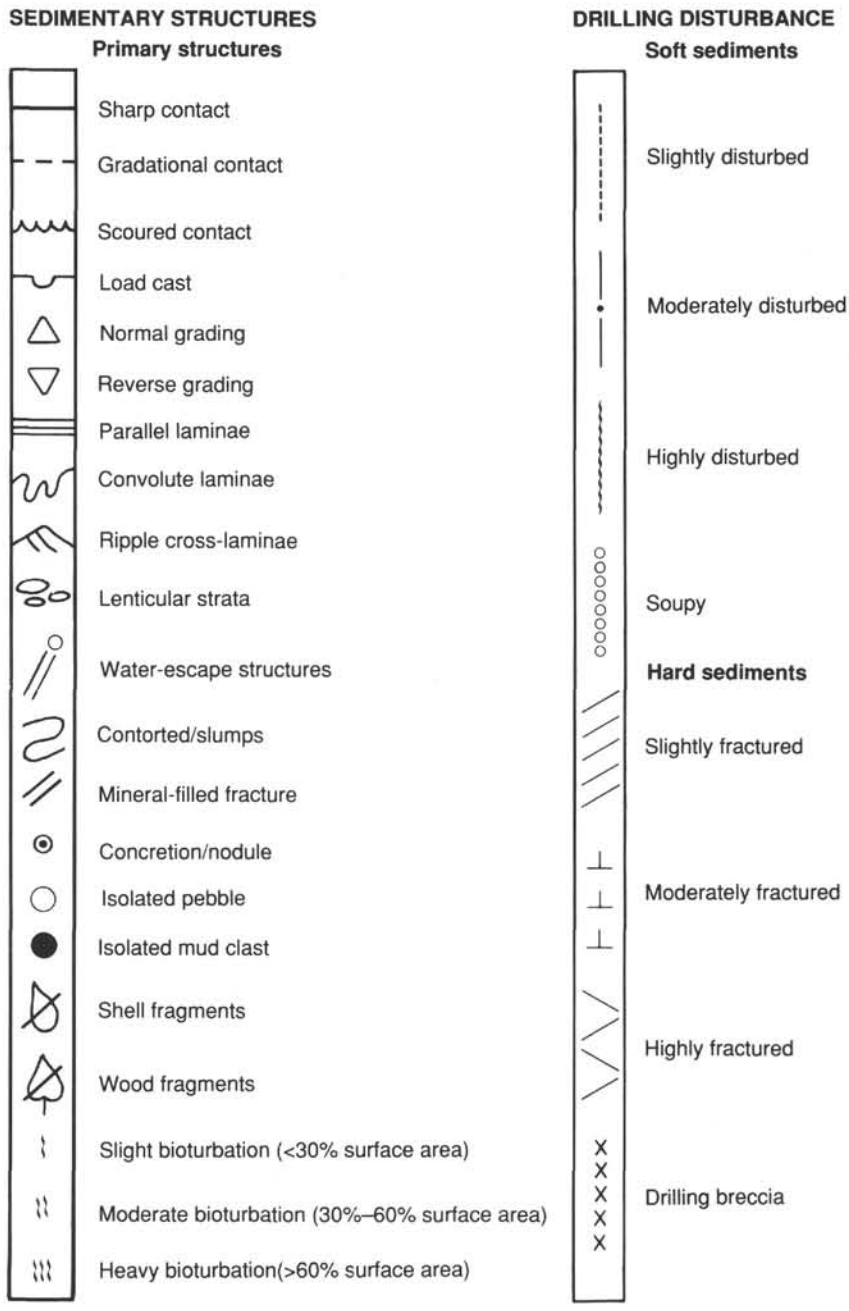

Figure 5. Symbols for drilling disturbance and sedimentary structure used on core description forms shown in Figure 3. Vertical arrows in the sediment structures column indicate the thickness of the interval over which a particular feature can be found.

appears in a separate part of the Explanatory Notes under the title "Structural Geology."

Turbidite Sedimentary Structures

In addition to using symbols to depict standard sedimentary structures, all turbidite deposits that contain well-defined internal sedimentary structures were classified during Leg 131 according to the Bouma sequence (Fig. 6). The basal T_a division of the Bouma sequence displays normal particle-size grading or structureless (massive) bedding. The T_b division comprises plane-parallel laminae, and the T_c division shows either convolute lamination or ripple cross-laminae. The T_d division also contains plane-parallel laminae, but these laminae generally are finer grained than those of the T_b division. Structureless turbiditic or hemipelagic mud makes up the T_e division. A complete Bouma sequence is abbreviated as $T_{a\text{-}e}$. It should be noted, however, that the Bouma sequence is actually an idealized composite, and most turbidites do not contain all of the designated internal sedimentary structures. By convention, we abbreviated partial sequences using subscripts to indicate the divisions that are present. For example, a T_{bce} bed begins with the T_b division (i.e., a base-cut-out turbidite) and passes into the T_c division; the T_d division is absent also, with the T_c division overlain directly by structureless mud.

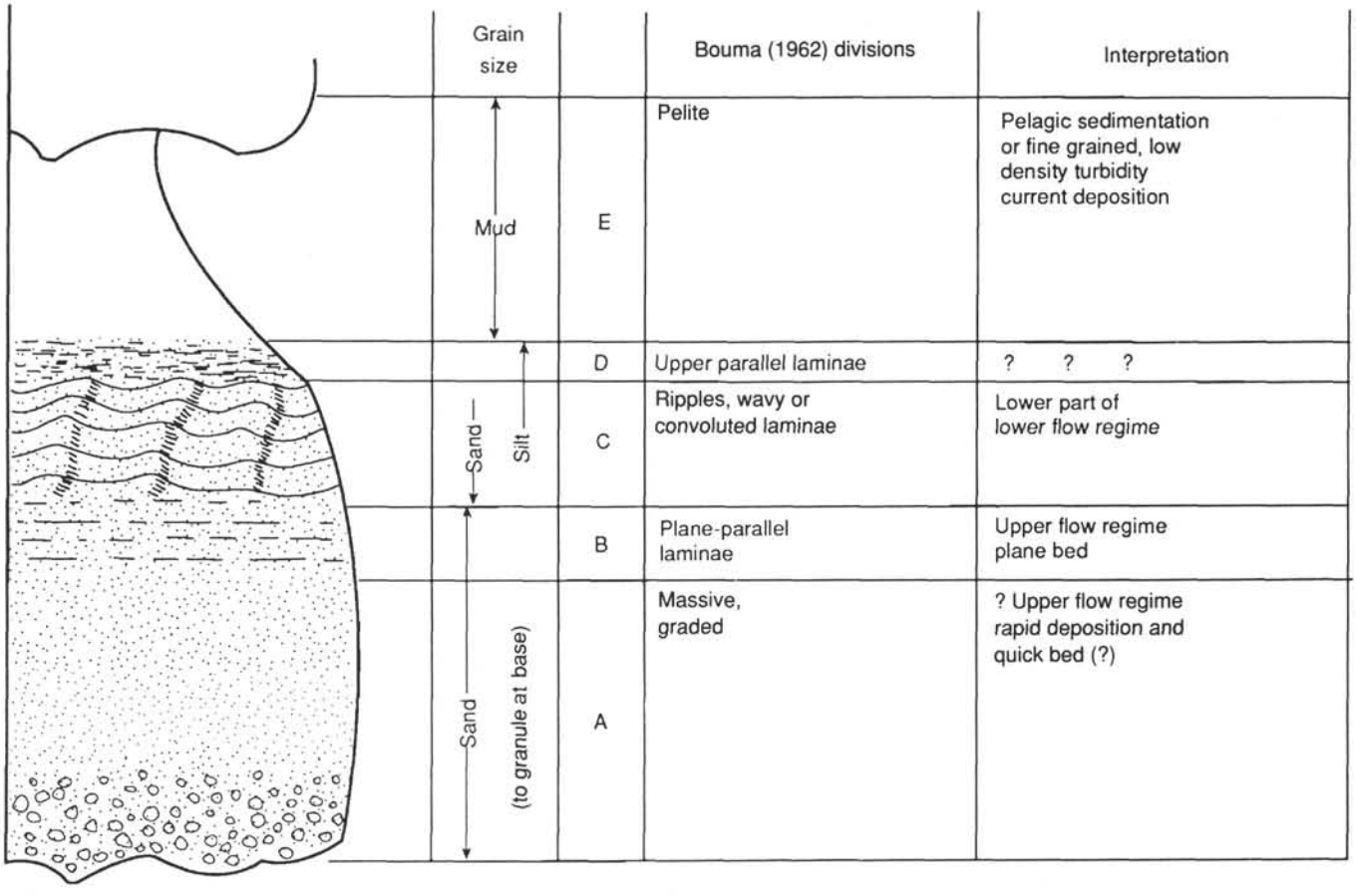

Figure 6. Graphical depiction of an idealized turbidite showing a complete Bouma sequence of internal sedimentary structures and corresponding hydrodynamic interpretations for each division (from Blatt et al., 1980).

Sediment Disturbance

Sediment disturbances that clearly result from the coring process, rather than from structural deformation, are illustrated in the "Drilling Disturbance" column on the core-description form (using the symbols shown in Fig. 5). Blank regions indicate a lack of drilling disturbance. Drilling disturbances for soft and firm sediments were categorized as follows:

1. Slightly deformed: bedding contacts are slightly bent.
2. Moderately deformed: bedding contacts show extreme bowing.
3. Highly deformed: bedding is completely disturbed and in some cases shows symmetric diapir-like or flow structures;
4. Soupy: intervals are water saturated and have lost all aspects of original bedding.

The degree of fracturing in indurated sediments and igneous rocks was described using the following categories:

1. Slightly fractured: core pieces are in place and contain little drilling slurry or breccia.
2. Moderately fragmented: core pieces are in place or partly displaced, but original orientation is preserved or recognizable (drilling slurry may surround fragments).
3. Highly fragmented: pieces are from the interval cored and probably in correct stratigraphic sequence (although they may not represent the entire section), but original orientation is completely lost.
4. Drilling breccia: core pieces have lost their original orientation and stratigraphic position and may be mixed with drilling slurry.

Induration

Subjective criteria were used during Leg 131 to determine the induration of muddy sediments. Three classes exist for the degree of induration:

1. Soft: sediments have little strength and are readily deformed under a finger or broad blade of a spatula.
2. Firm: partly lithified sediments are readily deformed under a fingernail or the edge of a spatula blade.
3. Hard: nonfriable, cemented or compacted rocks, with the suffix "-stone" added to the name (e.g., limestone, claystone).

Color

Colors were determined qualitatively by comparison with Munsell soil-color charts (Munsell Soil Color Charts, 1971). Colors were described immediately after the cores were split because redox-associated color changes may occur when deep-sea sediments are exposed to the atmosphere. Information on core colors is given in the text of the "Lithologic Description" on the core-description forms.

Samples

The positions of samples taken from each core for shipboard analysis are indicated in the "Samples" column of the core-description form (Fig. 3). The symbol "*" indicates the

locations of smear-slide samples, and the symbol "#" indicates the locations of thin-section samples. The notations "IW" and "OG" designate the locations of samples for whole-round interstitial water geochemistry and frozen organic geochemistry, respectively. Additional codes correspond to samples extracted by individual investigators. The notation "•" designates *fine-grained* intervals that were sampled both for shipboard measurements of physical properties and for grain-size distribution using the Lasentec particle-size analyzer (see following section on "Textural Analysis"). Any additional analyses of grain size that were run independently of the physical properties sample intervals are keyed to their location by the notation "+".

Smear-Slide Summary

A table summarizing data from smear slides and thin sections appears on each core-barrel description form. These tables include information on the sample location, whether the sample represents a dominant ("D") or a minor ("M") lithology in the core, and the estimated percentage ranges of sand, silt, and clay, together with all identified components. We emphasize here that smear-slide analyses provide only crude estimates of the relative abundances of detrital constituents; the mineralogies of finer-grained (silt-sized) particles are difficult to identify petrographically, and sand-sized grains tend to be underestimated because they cannot be incorporated into the smear evenly. In addition, estimates of grain size suffer from systematic errors because of differences between the surface areas of grains and their respective weight-percentages; this is particularly problematic with clay-sized particles. The following number codes represent the percentage ranges used: 1 = <2%; 2 = 2%–10%; 3 = 10%–25%; 4 = 25%–40%; and 5 = >40%.

Lithologic Description—Text

The lithologic descriptions that appear on each core-description form (barrel sheet) consist of two parts: (1) a heading that lists all the major sediment types in the core (see "Sediment Classification" section, this chapter); and (2) a more detailed description of these sediments, including data on color, stratal thickness, specific locations of key features in the core, geometries of diagnostic sedimentary structures, presence of Bouma divisions, and so on. The following terms were used to describe stratal thickness:

1. very thick bedded (>100 cm);
2. thick bedded (30–100 cm);
3. medium bedded (10–30 cm);
4. thin bedded (3–10 cm);
5. very thin bedded (1–3 cm).

Descriptions and locations of thin interbeds or minor lithologies also are included in the text.

SEDIMENTOLOGY

The sediment classification scheme for the Ocean Drilling Program (Mazzullo et al., 1987) was used during Leg 131. This classification defines two basic sediment types: (1) granular sediment and (2) chemical sediment.

Granular Sediment

Classes of Granular Sediment

Four grain types occur in granular sediments: pelagic, neritic, siliciclastic, and volcaniclastic. Their definitions are as follows:

1. Pelagic grains are fine-grained skeletal debris produced by open-marine siliceous and calcareous microfauna and microflora (e.g., radiolarians, nannofossils) and associated organisms.
2. Neritic grains are coarse-grained calcareous skeletal fragments (e.g., bioclasts, peloids) and fine-grained calcareous grains of nonpelagic origin.
3. Siliciclastic grains comprise minerals and rock fragments that were eroded from plutonic, sedimentary, and metamorphic rocks.
4. Volcaniclastic grains include glass shards, rock fragments, and mineral crystals that were produced by volcanic processes.

Variations in the relative proportions of these four grain types define five major classes of granular sediments: (1) pelagic, (2) neritic, (3) siliciclastic, (4) volcaniclastic, and (5) mixed sediments (Fig. 7). Pelagic sediments contain >60% pelagic plus neritic grains, <40% siliciclastic plus volcaniclastic grains, and a higher proportion of pelagic than neritic grains. Neritic sediments include >60% pelagic plus neritic grains, <40% siliciclastic plus volcaniclastic grains, and a higher proportion of neritic than pelagic grains. Siliciclastic sediments are composed of >60% siliciclastic plus volcaniclastic grains, <40% pelagic plus neritic grains, and they contain a higher proportion of siliciclastic than volcaniclastic grains. Volcaniclastic sediments contain >60% siliciclastic plus volcaniclastic grains, <40% pelagic and neritic grains, and a higher proportion of volcaniclastic than siliciclastic grains. This class includes epiclastic sediments (eroded from volcanic rocks by wind, water, or ice), pyroclastic sediments (products of explosive magma degassing), and hydroclastic sediments (granulation of volcanic glass by steam explosions). Lastly, mixed sediments are composed of 40%–60% siliciclastic plus volcaniclastic grains and 40%–60% pelagic plus neritic grains.

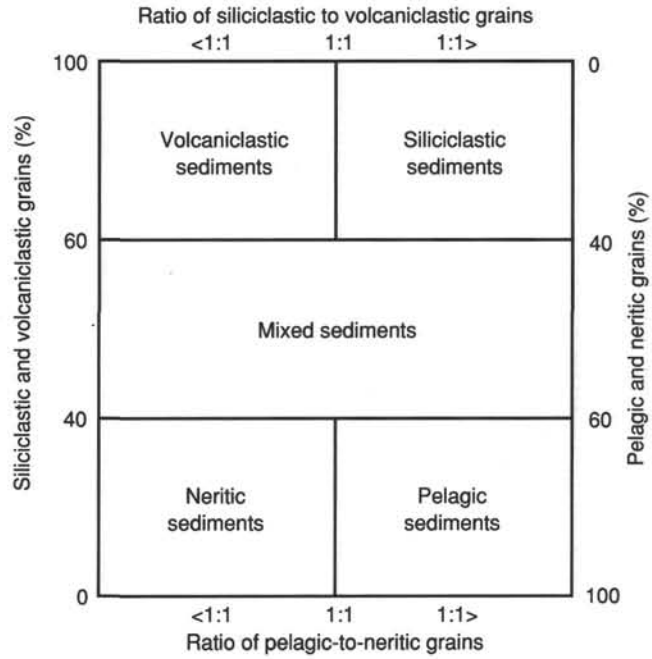

Figure 7. Diagram showing classes of granular sediment (modified from Mazzullo et al., 1987).

Classification of Granular Sediment

We classified granular sediment during Leg 131 by designating a principal name and major and minor modifiers. The principal name of a granular sediment defines its granular-sediment class; the major and minor modifiers describe the texture, composition, fabric, and/or roundness of the grains themselves (Table 1).

Principal Names

Each granular-sediment class has a unique set of principal names. For pelagic sediment, the principal name describes the composition and degree of consolidation using the following terms:

1. Ooze = unconsolidated calcareous and/or siliceous pelagic sediment;
2. Chalk = firm pelagic sediment composed predominantly of calcareous pelagic grains.
3. Limestone = hard pelagic sediment composed predominantly of calcareous pelagic grains.
4. Radiolarite, diatomite, and spiculite = firm pelagic sediment composed predominantly of siliceous radiolarians, diatoms, and sponge spicules, respectively.
5. Porcellanite = a well-indurated rock with abundant authigenic silica but less hard, lustrous, or brittle than chert (in part, such rocks may represent mixed sedimentary rock).
6. Chert = vitreous or lustrous, conchoidally fractured, highly indurated rock composed predominantly of authigenic silica.

For neritic sediment, the principal name describes the texture and fabric, using the Dunham (1962) classification for carbonate rocks. The following terms apply:

1. Boundstone = components organically bound during deposition;
2. Grainstone = grain-supported fabric, no mud, grains <2 mm in size;
3. Packstone = grain-supported fabric with intergranular mud, grains <2 mm in size.
4. Wackestone = mud-supported fabric with greater than 10% grains, grains <2 mm in size.
5. Mudstone = mud-supported fabric with less than 10% grains.
6. Floatstone = matrix-supported fabric, grains >2 mm in size.
7. Rudstone = grain-supported fabric, grains >2 mm in size.

For siliciclastic sediment, texture provides the main criterion for selection of a principal name. The Udden-Wentworth grain-size scale (Fig. 8) defines the grain-size ranges and the names of the textural groups (gravel, sand, silt, and clay) and subgroups (fine sand, coarse silt, etc.). Where two or more textural groups

Table 1. Outline of granular-sediment classification scheme (modified from Mazzullo et al., 1987).

Sediment class	Major modifiers	Principal names	Minor modifiers
Pelagic Sediment	1. composition of pelagic and calciclastic grains present in major amounts 2. texture of clastic grains present in major amounts	1. ooze 2. chalk 3. limestone 4. radiolarite 5. diatomite 6. spiculite 7. chert	1. composition of pelagic and neritic grains present in minor amounts 2. texture of clastic grains present in minor amounts
Neritic Sediment	1. compostition of neritic and pelagic grains present in major amounts 2. texture of clastic grains present in major amounts	1. boundstone 2. grainstone 3. packstone 4. wackestone 5. mudstone 6. floatstone 7. rudstone	1. composition of neritic and pelagic grains present in minor amounts 2. texture of clastic grains present in minor amounts
Siliciclastic Sediment	1. composition of all grains present in major amounts 2. grain fabric (gravels only) 3. grain shape (optional) 4. sediment color (optional)	1. gravel 2. sand 3. silt 4. clay (etc.)	1. composition of all grains present in minor amounts 2. texture and composition of siliciclastic grains present as matrix (for coarse-grained clastic sediments)
Volcaniclastic Sediment	1. composition of all volcaniclasts present in major amounts 2. composition of all pelagic and grains present in major amounts 3. texture of siliciclastic grains present in major amounts	1. breccia 2. lapilli 3. coarse ash/tuff 4. fine ash/tuff	1. composition of all volcaniclasts present in minor amounts 2. composition of all neritic and pelagic grains present in minor amounts 3. texture of siliciclastic grains present in minor amounts
Mixed Sediment	1. composition of neritic and pelagic grains present in major amounts 2. texture of clastic grains present in major amounts	1. mixed sediments 2. marl/ marlstone	1. composition of neritic and pelagic grains present in minor amounts 2. texture of clastic grains present in minor amounts

	U.S. Standard sieve mesh	Millimeters	Phi (ϕ) units	Wentworth size class
GRAVEL	Use wire squares	4096	−12	
		1024	−10	Boulder
		256	256 −8	
		64	64 −6	Cobble
		16	−4	Pebble
	5	4	4 −2	
	6	3.36	−1.75	
	7	2.83	−1.5	Granule
	8	2.38	−1.25	
	10	2.00	2 −1.0	
SAND	12	1.68	−0.75	
	14	1.41	−0.5	Very coarse sand
	16	1.19	−0.25	
	18	1.00	1 0.0	
	20	0.84	0.25	
	25	0.71	0.5	Coarse sand
	30	0.59	0.75	
	35	0.50	1/2 1.0	
	40	0.42	1.25	
	45	0.35	1.5	Medium sand
	50	0.30	1.75	
	60	0.25	1/4 2.0	
	70	0.210	2.25	
	80	0.177	2.5	Fine sand
	100	0.149	2.75	
	120	0.125	1/8 3.0	
	140	0.105	3.25	
	170	0.088	3.5	Very fine sand
	200	0.074	3.75	
	230	0.0625	1/16 4.0	
SILT	270	0.053	4.25	
	325	0.044	4.5	Coarse silt
		0.037	4.75	
		0.031	1/32 5.0	
		0.0156	1/64 6.0	Medium silt
	Use	0.0078	1/128 7.0	Fine silt
	pipette	0.0039	1/256 8.0	Very fine silt
MUD	or hydrometer	0.0020	9.0	
		0.00098	10.0	Clay
		0.00049	11.0	
		0.00024	12.0	
		0.00012	13.0	
		0.00006	14.0	

Figure 8. Udden-Wentworth grain-size scale (in mm) for siliciclastic sediments, together with comparable values in Phi units and standard sieve mesh sizes (from Pettijohn et al., 1973).

or subgroups are present, the principal names appear in order of increasing abundance. Ten major textural categories can be defined on the basis of relative proportions of sand, silt, and clay (Fig. 9). However, in practice, distinctions between some of the categories are dubious without accurate measurements of weight percentages. This is particularly true for the boundary between silty clay and clayey silt. The suffix "-stone" is affixed to the principal names sand, silt, and clay when the sediment is lithified. The terms "conglomerate" and "breccia" are the principal names of gravels with well-rounded and angular clasts, respectively.

For volcaniclastic sediment, the principal name is also dictated by the texture. The names and ranges of three textural groups (from Fisher and Schmincke, 1984) are as follows:

1. Volcanic breccia = pyroclasts greater than 64 mm in diameter.
2. Volcanic lapilli = pyroclasts between 2 and 64 mm in diameter (when lithified, the term "lapillistone" is used).
3. Volcanic ash = pyroclasts less than 2 mm in diameter (when lithified, the term "tuff" is used).

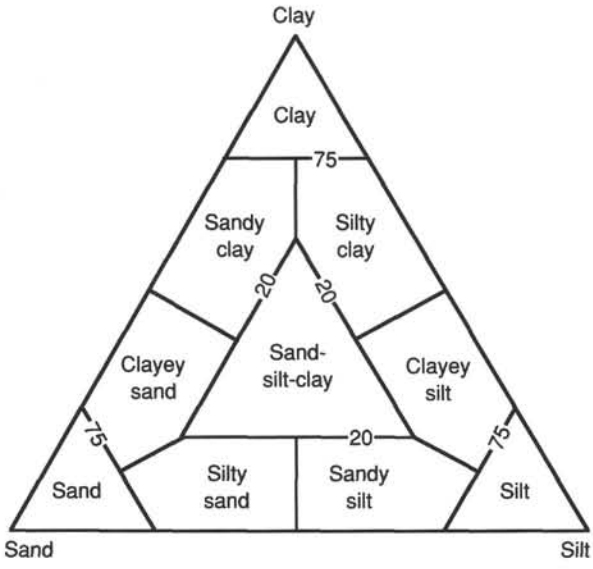

Figure 9. Ternary diagram showing classification scheme for siliciclastic sediments and sedimentary rocks. Classification is modified from Shepard (1954).

For mixed sediment, the principal name describes the degree of consolidation, with the term "mixed sediment" used for unlithified sediment and the term "mixed sedimentary rock" used for lithified sediment.

Major and Minor Modifiers

To describe the lithology of the granular sediment in greater detail the principal name of a granular-sediment class is preceded by major modifiers and followed by minor modifiers (Table 1). Minor modifiers are preceded by the term "with." The most common uses of major and minor modifiers are to describe the composition and textures of grain types that are present in major (greater than 25%) and minor (10%–25%) proportions. In addition, major modifiers can be used to describe grain fabric, grain shape, and sediment color.

The composition of pelagic grains can be described in greater detail with the major and minor modifiers diatom(-aceous), radiolarian, spicules(-ar), siliceous, nannofossil, foraminifer(-al), and calcareous. The terms siliceous and calcareous are used to describe sediments that are composed of siliceous or calcareous pelagic grains of uncertain origin.

The compositional terms for neritic grains include the following major and minor modifiers:

1. Ooid (or oolite) = spherical or elliptical nonskeletal particles smaller than 2 mm in diameter, having a central nucleus surrounded by a rim with concentric or radial fabric.
2. Bioclast (or bioclastite) = fragment of skeletal remains (specific names such as molluscan or algal can also be used).
3. Pellet (-al) = fecal particles from deposit-feeding organisms.
4. Intraclast = reworked carbonate-rock fragment or rip-up clast.
5. Pisolite = spherical or ellipsoidal nonskeletal particle, commonly greater than 2 mm in diameter, with or without a central nucleus but displaying multiple concentric layers of carbonate.
6. Peloid (pel) = micritized carbonate particle of unknown origin.
7. Calcareous, dolomitic, aragonitic, sideritic = the mineral composition of carbonate muds or mudstones (micrite) of nonpelagic origins.

The textural designations for siliciclastic grains utilize standard major and minor modifiers such as gravel(-ly), sand(-y), silt(-y), and clay(-ey). The character of siliciclastic grains can be described further by mineralogy (using modifiers such as "quartz," "feldspar," "glauconite," "mica," "kaolinite," "zeolitic," "lithic," "calcareous," "gypsiferous," or "sapropelic." In addition, the provenance of rock fragments (particularly in gravels, conglomerates, and breccias) can be described by modifiers such as volcanic, sed-lithic, meta-lithic, gneissic, and plutonic. The fabric of a sediment can be described as well using major modifiers such as grain-supported, matrix-supported, and imbricated. Generally, fabric terms are useful only when describing gravels, conglomerates, and breccias.

The composition of volcaniclastic grains is described by the major and minor modifiers "lithic" (rock fragments), "vitric" (glass and pumice), and "crystal" (mineral crystals). Modifiers can also be used to describe the compositions of the lithic grains and crystals (e.g., feldspathic or basaltic).

Chemical Sediments

Classes of Chemical Sediment

Chemical sediments are composed of minerals that formed by inorganic processes such as precipitation from solution or colloidal suspension, deposition of insoluble precipitates, or recrystallization. Chemical sediments generally have a crystalline (i.e., nongranular) texture. There are five classes of chemical sediments: (1) carbonaceous sediments, (2) evaporites, (3) silicates, (4) carbonates, and (5) metalliferous sediments. Chemical sediments were not encountered on Leg 131, but brief descriptions are included below.

Carbonaceous sediments contain >50% organic matter (plant and algal remains) that has been altered from its original form by carbonization, bituminization, or putrification. Examples of carbonaceous sediments include peat, coal, and sapropel (jelly-like ooze or sludge of algal remains). The evaporites are classified according to their mineralogy using terms such as halite, gypsum, and anhydrite. They may be modified by terms that describe their structure or fabric, such as massive, nodular, and nodular-mosaic. Silicates and carbonates are defined as crystalline sedimentary rocks that are nongranular and nonbiogenic in appearance. They are classified according to their mineralogy, using principal names such as chert (microcrystalline quartz), calcite, and dolomite. They should also be modified with terms that describe their crystalline (as opposed to granular) nature, such as crystalline, microcrystalline, massive, and amorphous. Metalliferous sediments are nongranular, nonbiogenic sedimentary rocks that contain metal-bearing minerals such as pyrite, goethite, manganese, chamosite, and glauconite. They are classified according to their mineralogy.

Textural Analyses

Semiquantitative shipboard analyses of sediment texture were completed on muddy specimens only, using a Lasentec LAB-TEC 100 particle-size analyzer. This system uses a focused laser beam that sweeps across particles suspended in a solution. The instrument measures the back-scattering of light, which means that particle sizes can be measured at relatively high concentration levels.

Sample preparation during Leg 131 involved complete disaggregation of the specimen (approximately 1 cm^3) in 30 mL of distilled water and 20 mL of sodium hexametaphos-

phate (Calgon) solution; the Calgon solution (concentration = 4 g/L) was added to prevent flocculation of clay minerals. For moderately compacted samples, the disaggregation was aided by a mechanical shaker and 2–3 min of immersion in an ultrasonic bath. Longer durations (up to 30 min) of ultrasonic treatment and agitation with a magnetic stirrer were required for harder specimens. Even with these treatments, however, percentages of clay-sized particles are probably seriously underestimated for indurated specimens.

Sediment particles are held in suspension during the grain-size analysis by a magnetic stirring bar; data for specimens containing large percentages of coarse silt and sand are unreliable because of the inability of the stirring bar to maintain grain suspension up to the level of the laser beam. Scanning times per count were set at 1 s, and the grain-shape factor was set at 66.7 (with 0 equivalent to a perfectly smooth sphere and 100 equivalent to a very rough surface and irregular shape).

The particle-size analyzer counts the number of individual grains that fall into given size-range categories, and compensation factors must be applied to convert the raw count data to percent-by-weight readings. The following eight grain-size ranges (in micrometers) were recorded: >125, 125–62, 62–31, 31–16, 16–8, 8–4, 4–2, and <2. Compensation factors were set at the mid-points of each grain-size range. Graphic output was obtained using a percent-per-channel (histogram) mode. Calculations of mean grain size were also made automatically. A test of reproducibility showed that the standard deviation for values of mean grain size is equal to approximately 1.4 μm; this test involved an indurated sample (to maximize the problems with complete disaggregation) and 15 separate runs.

Whenever possible, the grain-size distributions were used to help place textural descriptions within the Shepard (1954) textural classification (Fig. 9). However, because of inaccurate readings at the upper and lower ends of the grain-size range, and because grain standards were not available to calibrate the machine (particularly the weight-% compensation factors and grain-shape correction), the results simply serve as a measure of relative changes in grain-size distribution rather than absolute values. Additional discussion of the use of this machine can be found in the Explanatory Notes for ODP Leg 124 (Shipboard Scientific Party, 1990).

X-Ray Diffraction

The mineralogy and relative abundances of common minerals were analyzed on bulk samples using X-ray diffraction techniques. Bulk samples were freeze-dried, ground to a fine powder with a mortar and pestle, then packed into aluminum holders. The randomly oriented powders were not treated with any chemicals.

The X-ray laboratory aboard the *JOIDES Resolution* is equipped with a Phillips PW-1729 X-ray generator, a Phillips PW-1710/00 diffraction control unit with a PW-1775 35-port automatic sample changer, and a Phillips PM-8151 digital plotter. Machine parameters were set as follows: generator = 40 kV and 35 mA; tube anode = Cu; wavelength = 1.5405620 Å ($CuK\alpha_1$) and 1.5443900Å ($CuK\alpha_2$); intensity ratio = 0.5; focus = fine; divergence slit = 12.5 mm; receiving slit = 0.2 mm; step size = 0.020°2Θ; count time = 1 s; scanning rate = 2°2Θ/min; rate meter time constant = 0.2 s; spinner = off; monochrometer = on; scan = continuous; scanning range = 2°2-60°2Θ. Output of the digital data includes the angular position of each peak (°2Θ), the corresponding d-spacing (Å), counts above background (cycles per second), and the individual peak intensities expressed as percentages of the maximum intensity (100); the maximum intensity is usually produced by quartz. Interpretations of the X-ray data also utilized graphics output; the graphics terminal produces continuous tracings of the diffraction peaks expressed in terms of cycles per second above background counts. Because of peak drift due to slight variations in the alignment of individual sample holders using the automatic changer, all peak positions were corrected relative to the shift of the highest intensity quartz peak (26.65°2Θ).

In addition to the routine identification of detrital and diagenetic minerals, we estimated relative abundances of dominant minerals by applying correction factors to the peak intensities and normalizing those weighted values to 100%. We selected the weighting factors established by Cook et al. (1975), who completed calibration experiments using 50:50 mixtures of given mineral standards plus quartz. Diagnostic peak positions and the corresponding intensity factors are listed in Table 2. Relative percentages of total clay, quartz, plagioclase, and calcite were calculated in this manner.

Each relative percentage of total clay is based on the sum of the weighted intensities of four individual clay minerals: smectite, illite, kaolinite, and chlorite. Relative percentages of each clay mineral can be calculated also, in theory, but because the peak intensities for the clay minerals tend to be small in bulk powders, the potential errors associated with such calculations are large. In addition, the diagnostic kaolinite peak interferes with a chlorite peak at approximately 12.46°2Θ; consequently, the weighted-intensity value reported for chlorite is based upon the peak that occurs at approximately 18.80°2Θ, and the weighted-intensity value for chlorite then must be subtracted from the weighted-intensity value of kaolinite+chlorite. Weighted intensities for kaolinite were set at 0 if the weighted chlorite value turned out to be greater than the weighted value of kaolinite+chlorite.

Thin-Section Petrography

Detrital modes for turbidite sands were calculated based upon point counts of unstained thin sections. Sand samples first were washed using a 0.063-mm screen, then freeze-dried, mixed with epoxy, and cut into standard thin sections. Counts were limited to 300 grains from the modal categories listed in Table 3, plus any additional grains encountered (listed under the heading of minor constituents). To reduce the possible effects of variable grain size on modal data, only aphanitic grains have been assigned to the polycrystalline headings; sand-sized phenocrysts in volcanic rock fragments and sand-sized grains within sedimentary and plutonic aggregates are included with their mono-mineralic kin.

BIOSTRATIGRAPHY

Preliminary age assignments were primarily established based on core-catcher samples. Samples from within the cores were examined when a refined age determination was necessary. Two microfossil groups were examined for biostratigraphic purposes: calcareous nannofossils and radiolarians. Sample positions and the abundance, preservation, and age or zone for each fossil group is recorded on barrel sheets for each core.

Table 2. Peak positions and d-spacings for common minerals analyzed by X-ray diffraction, with associated intensity factors as determined by Cook et al. (1975).

Mineral	Window (°2Θ)	D-Spacing (Å)	Intensity Factor
Calcite	29.25–29.60	3.05–3.01	1.65
Chlorite	18.50–19.10	4.79–4.64	4.95
Kaolinite	12.39–12.60	7.14–7.02	2.25
Illite	8.75–9.10	10.10–9.72	6.00
Plagioclase	27.80–28.15	3.21–3.17	2.80
Quartz	26.65	3.34	1.00
Smectite	5.73–6.31	15.42–14.01	3.00

Table 3. Detrital modes and minor constituents in turbidite sands.

DETRITAL MODES	
Q_m	= monocrystalline quartz + sand-sized aggregates
Q_p	= microcrystalline + cryptocrystalline quartz
Q	= $Q_m + Q_p$
F	= plagioclase + K-feldspar (including sand-sized phenocrysts)
V_g	= volcanic glass shards
V_r	= aphanitic volcanic rock fragments
L_v	= $V_g + V_r$
L_s	= sedimentary rock fragments (shale, siltstone, claystone)
L_m	= metasedimentary rock fragments (slate, phyllite, schist)
L_{sm}	= $L_s + L_m$
L	= $L_v + L_s + L_m$
MINOR CONSTITUENTS	
H	= heavy minerals (pyroxene, amphibole, chlorite, etc.)
C	= biogenic carbonate
M	= mica
O	= others, unknowns, opaque, or altered beyond recognition

The time scale by Berggren et al. (1985a, 1985b) was used for the Cenozoic. Tables 4 and 5 summarize the nannofossil and radiolarian datums, respectively, used for Leg 131.

Calcareous Nannofossils

Because the age range of the sediments penetrated on this leg is from Holocene to Miocene, the classification of Leg 131 sediments is expressed by the use of a single Neogene zonal scheme.

Chronological Framework

The age estimates of Cenozoic calcareous nannofossil zonal boundaries have largely been derived from the geomagnetic polarity time-scale (GPTS) of Berggren et al. (1985a, 1985b). A few age estimates shown in Table 4 are taken directly from Berggren et al. (1985b), however more recent improved correlations between nannofossil biostratigraphy and the GPTS account for most of the age estimates.

Cenozoic Zonation

The Cenozoic nannofossil zonation of Martini (1971) was used for Leg 131 sediments. We have, however, also used numerous biostratigraphic events that are not used in Martini's (1971) zonal boundary definitions (Table 4). These additional events provide substantially improved biostratigraphic and biochronological resolution.

Methods

Smear slides were prepared for each sample, using either Ayal or Norland Optical Adhesive as a mounting medium. The calcareous nannofossils were examined in smear slides by standard light microscopy techniques (plane- polarized light, phase-contrast or cross-polarized light at approximately ×790, or ×1250, magnification).

Calcareous nannofossils often show signs of both strong etching and strong overgrowth; more dissolution-resistant forms add secondary calcite provided by more dissolution-prone morphotypes. We have adopted a simple code system for characterizing preservational states. Preservation was recorded using one of the three following letter designations:

G = good (little or no evidence of dissolution and/or secondary overgrowth of calcite, diagnostic characteristics fully preserved).

M = moderate (dissolution and/or secondary overgrowth partially alter primary morphological characteristics, but nearly all specimens can be identified at the species level).

P = poor (severe dissolution, fragmentation and/or secondary overgrowth with primary features largely destroyed, many specimens cannot be identified at the species and/or generic level).

Abundance estimates of the nannofossils in the smear slides were made on optimum density areas of the slide, that is, areas where most of the field was covered with sample material without appreciable piling of specimens or sample

Table 4. Calcareous nannofossil datum events used in Leg 131.

Event	Species	Zone (top)	Age (Ma)	References
OA	*Emiliania huxleyi*		0.09	1
FO	*Emiliania huxleyi*	NN20	0.28	1
LO	*Pseudoemiliania lacunosa*	NN19	0.46	1
LO	*Reticulofenestra asanoi*		0.83	2
FO	*Gephyrocapsa parallela*		0.83	2
TA	small *Gephyrocapsa*		0.94	4
FO	*Reticulofenestra asanoi*		1.06	2
LO	large *Gephyrocapsa* (>5.5 μm)		1.10	2
OA	small *Gephyrocapsa*		1.14	4
LO	*Helicosphaera sellii*		1.19	2
FO	large *Gephyrocapsa* (>5.5μm)		1.36	2
LO	*Calcidiscus macintyrei*		1.45(1.57)	3(2)
FO	*Gephyrocapsa oceanica*		1.57	2
FO	*Gephyrocapsa caribbeanica*		1.66	2
Pleistocene/Pliocene boundary			1.66	4
LO	*Discoaster brouweri*	NN18	1.89	3
LO	*Discoaster triradiatus*		1.89	3
AS	*D. triradiatus/D. brouweri*		2.01	4
OA	*Discoaster triradiatus*		2.07	5
LO	*Discoaster asymmetricus*		2.20	6b
LO	*Discoaster pentaradiatus*	NN17	2.35	3
LO	*Discoaster surculus*	NN16	2.41	3
LO	*Discoaster tamalis*		2.65	3
FO	*Pseudoemiliania lacunosa*		3.40	6b
LO	*Sphenolithus* spp.		3.45	3
LO	*Sphenolithus abies/neoabies*		3.47	6b
LO	*Reticulofenestra pseudoumbilica*	NN15	3.56	3
LO	*Amaurolithus tricorniculatus*	NN14	3.7	6a
FO	*Discoaster asymmetricus*	NN13	4.1	6a
LO	*Amaurolithus primus*		4.4	6a
FO	*Ceratolithus rugosus*	NN12	4.6	3
LO	*Ceratolithus acutus*		4.6	3
FO	*Ceratolithus acutus*		4.9	7
LO	*Triquetrorhabdulus rugosus*		4.9	7
Pliocene/Miocene boundary			4.9	8
LO	*Discoaster quinqueramus*	NN11	5.0	7
LO	*Amaurolithus amplificus*		5.4	9
FO	*Amaurolithus amplificus*		6.0	9
FO	*Amaurolithus primus*		6.7	9
FO	*Discoaster quinqueramus*	NN10	7.5	7
FO	*Discoaster berggrenii*		8.2	6a
LO	*Discoaster hamatus*	NN9	8.7	7
LO	*Catinaster* spp.		8.8	7
FO	*Discoaster neohamatus*		9.0	7
FO	*Catinaster calyculus*		10.0	6a
FO	*Discoaster hamatus*	NN8	10.5	7
FO	*Catinaster coalitus*	NN7	11.1	7
FO	*Discoaster kugleri*	NN6	12.2	7
LO	*Coronocyclus nitescens*		12.8	9
LO	*Cyclicargolithus floridanus*		13.1	7
LO	*Sphenolithus heteromorphus*	NN5	13.6	7
LO	*Helicosphaera ampliaperta*	NN4	16.0	6a
TA	*Discoaster deflandrei* group		16.1	9
FO	*Sphenolithus heteromorphus*		18.6	7
LO	*Sphenolithus belemnos*	NN3	18.8	7
LO	*Triquetrorhabdulus carinatus*	NN2	19.5	7
FO	*Sphenolithus belemnos*		20.0	7
FO	*Discoaster druggii*	NN1	23.6	7
TA	*Sphenolithus delphix*		23.6	10
Miocene/Oligocene boundary			23.7	6a

Acronyms used: FO = first occurrence; LO = last occurrence; OA = onset acme; TA = termination acme; AS = abundance shift.
Zonal codes are those of Martini (1971).
Age column references represent: (1) Thierstein et al., 1977; (2) Sato et al., in press; (3) Backman and Shackleton, 1983; (4) Rio et al., *in* press; (5) Backman and Pestiaux, 1986; (6a) Berggren et al., 1985a; (6b) Berggren et al., 1985b; (7) Backman et al., 1990; (8) Zijderveld et al., 1986; (9) Rio et al., 1990; (10) Fornaciari et al., 1990.

Table 5. Tropical Cenozoic radiolarian zonation and species events used in Leg 131. Species events are based on Sanfilippo et al. (1985), Prell, Niitsuma, et al. (1989) and Johnson and Nigrini (1985).

Zone	Age	Top or bottom	Species
B. invaginata			
		B	*Buccinosphaera invaginata*
C. tuberosa	0.37–0.47	T	*Axoprunum angelinum*
	0.40–0.59	B	*Collospaera tuberosa*
A. ypsilon	0.76–0.84	B	*Pterocorys hertwigii*
	1.0–1.4	T	*Anthocyrtidium nosicaae*
	0.94–1.04	T	*Anthocyrtidium angulare*
	1.02–1.07	B	*Lamprocyrtis nigriniae*
A. angulare	1.09–1.13	T	*Lamprocyrtis neoheteroporos*
	1.52–1.56	T	*Pterocanium prismatium*
	1.52–1.64	B	*Anthocyrtidium angulare*
	2.42–2.44	T	*Theocalyptra davisiana*
P. prismatium	2.51–2.53	B	*Lamprocyrtis neoheteroporus*
	2.62–2.64	T	*Stichocorys peregrina*
	3.26–3.28	T	*Phormostichoartus fistula*
	3.33–3.35	T	*Lychnodictyum audax*
	3.53–3.55	T	*Phormostichoartus doliolum*
	3.77–3.79	B	*Amphirhopalum ypsilon*
S. pentas	3.74–3.82	T	*Spongaster pentas*
	3.83–3.85	B	*Spongaster tetras tetras*
	3.85–3.87	T	*S. berminghami*
	4.7–5.1		*S. berminghami -> S. pentas*
	4.4–4.7	B	*S. pentas*
S. peregrina	4.3–4.6	T	*Solenosphaera omnitubus*
	5.0–5.1	T	*Siphostichartus corona*
	5.2–5.3	T	*Acrobotrys tritubus*
	5.7–5.8	T	*Stichocorys johnsoni*
	5.9–6.2		*S. delmontensis -> S. peregrina*
	6.4–6.8	B	*Solenosphaera omnitubus*
D. penultima			*D.antepenultima -> D. penultima*
	6.9–7.1	T	*Diartus hughesi*
	7.7–7.9	B	*Acrobotrys tritubus*
D. antepenultima	8.0–8.3	T	*Botryostrobus miralestensis*
	8.1–8.4	T	*Diartus pettersoni*
	8.2–8.5		*D. pettersoni -> D. hughesi*
	7.9–8.0	B	*Spongaster berminghami*
	8.1–8.2	T	*Stichocorys wolffii*
	10.0–10.3	T	*Cyrtocapsella japonica*
		T	*Lithopera thornburgi*
D. pettersoni	11.8–12.1	T	*Cyrtocapsella tetrapera*
	11.4–11.5	T	*Cyrtocapsella cornuta*
		B	*Phormostichoartus doliolum*
		T	*Dorcadospyris altata*
		B	*Diartus petterssoni*
			L. renze -> L. neotera
		B	*Lithopera thornburgi*
		B	*Phormostichoartus corbula*
D. altata	13.7–13.8	T	*Calocycletta virginis*
	14.5–14.6	T	*Calocycletta costata*
		T	*Didymocyrtis violina*
		T	*Didymocyrtis tubaria*
		B	*Lithopera renzae*
		T	*Dorcadospyris forcipata*
			D. dentata -> D. altata

material. Four different levels of relative abundances, similar to the format outlined by Hay (1970), are defined as follows:

A = abundant: >10% (usually more than 10 specimens per viewfield).

C = common: 1%–10% (1 to 10 specimens per viewfield).

F = few: 0.1%–1% (1 specimen per 1 to 10 viewfields).

R = rare: <0.1% (only 1 specimen in more than 10 viewfields).

Radiolarians

Zonation

Radiolarian zonal assignments of Cenozoic samples were based on the tropical zonation of Riedel and Sanfilippo (1978) and subsequent modification in Sanfilippo et al. (1985). Table 5 shows the radiolarian species events used to establish a biochronology for Leg 131. Ages used are from previous data (Johnson and Nigrini, 1985; Nigrini and Caulet, 1988; Prell, Niitsuma, et al., 1989).

Abundance

Total abundance of radiolarians was estimated on strewn slides of sieved residues. Abundance was recorded on the Core-Description forms as follows:

A = abundant (>1000 radiolarians per slide)

C = common (101–1000 radiolarians per slide)

F = few (11–101 radiolarians per slide)

R = rare (1–11 radiolarians per slide)

B = barren

Preservation

Preservation of radiolarian tests in strewn slides was defined as follows:

G = good (little or no evidence of dissolution and/or fragmentation, diagnostic characteristics fully preserved).

M = moderate (dissolution and/or fragmentation partially alter primary morphological characteristics, but nearly all specimens can be identified at the species level).

P = poor (severe dissolution and/or fragmentation with primary features largely destroyed, many specimens cannot be identified at the species and/or generic level).

Sample Preparation

All samples examined in this study were treated in the following manner: about 5 cm^3 of each sample were boiled in 2% calgon solution for 5 to 20 minutes, and then were sieved and the fraction >38 μm was examined. Carbonate-rich samples were first decalcified in 10% hydrochloric acid. The residues including radiolarians tests were mounted in Entellan New mounting medium and observed under a transmitted-light microscope.

STRUCTURAL GEOLOGY

Introduction

An understanding of the structural geology of the Nankai accretionary prism was one of the prime objectives of Leg 131. Knowledge of the structures present is necessary for understanding the configuration of the prism and the deformation processes that are operating, as well as providing a link between the stratigraphy, physical properties, and the other aspects that were investigated on the leg. The deformation structures may well be central to an explanation of the fluid-flow characteristics of the prism.

With such things in mind, an effort was made to document every structure that was recovered, and to record it in as consistent and quantitative a way as possible. Apart from the whole-round samples that had to be taken immediately after core recovery, all material was examined for structural features. The next section of this chapter describes a simple instrument that we found extremely helpful in making accurate measurements of the structures. With a relatively large part of this leg being devoted to activities other than coring, and having a team of four structural geologists, it was possible to document the structures thoroughly, so that the various statistical treatments presented in this volume are reasonably meaningful.

A working core description form was devised, together with a spreadsheet that allowed computer manipulation and storage of the data. The layout of both forms evolved during usage; examples of the final versions are illustrated in Figures 10 and 11. Future improvements to the spreadsheet would

ODP CORE DESCRIPTION: STRUCTURAL GEOLOGY LEG 131 SITE 808 HOLE C CORE 38R COMMENTS SOME FRACTURES, BUT MAINLY GOOD, INTACT PIECES, ~10cm LONG.

SECTION (1 - 6)	INTERVAL (top-bottom, cm)	IDENTIFIER (see foot of page)	DIPS (apparent/true; 0-90, + or -)	AZIMUTHS (core work) STRIKE/TREND (North corrected)	PALEOMAG. (declin. / inclin.)	FAULTS (N,R,S,D, displ.)	COMMENTS AND SKETCHES
	3	BEDDING	05 – TRUE	[180/05W]	D=315, I=65, mag north =135		HOMOGENEOUS, BIOTURBATED MUDS. LITTLE OVERALL DEFORMATION.
25-150cm struc. continuous	28	FRACTURE	21 –	(33 towards 180), slicks trend 090.		displ. unknown	working azimuth: [121/37S]
	47	"	23–	(22 towards 180) " 083		"	[13E/30E]
1	67-73	FAULT	13 –	[252/73N]		NORMAL	unorganized recent fractures
	67	SHEAR BAND	47+ TRUE	[000/47E]			core edge
	82	FAULT	13–	(10 towards 180) slicks 065		—	bioturb.
	85 – 90	BEDDING	03 –	(07 " 000)			
	99	SHEAR BAND	00 TRUE				
0-22 struc. cont.	2	FAULT	84 +	007		NORMAL	[007/84E]
	30	BEDDING	8 –	189			thin dark laminae among bioturb. [189/08W]
22-150 struc. cont.	40-55	FAULT	62 +	(37 tow. 000)	22-150cm	NORMAL	[338/64E]
		"	66+	(38 tow. 000)	D=320	" , 0.8cm	[341/67E]
	74	FAULT	73–	(63 tow. 180)	I=46	" , 0.2cm	down-dip slickenlines [149/75W]
2	"	"	62–	(50 tow. 180)	mag. N =140	" , 0.3cm	[148/66W]
	76	FAULT	70 –	(42 tow. 180)			cut by fault at 82cm.
	76	BEDDING	05 – TRUE	[180/05W]			
	82	FAULT	22+	(19 tow. 000) [320/28E]			slicks trend 090 [27/090]
	83	"	27+	(03 tow. 180) [006/27E]			narrow zones of dark material, truncate burrows, etc.
	122	"	18+	(33 tow. 180) [063/36S]			prob. little displacement
0-150 struc. continuous piece	20	BEDDING	03–	(07 tow. 000) [247/08N]	0-150cm D=310 with reversal in centre mag N: 130		aligned bioturb. casts + dark clays.
	87	FAULT	15+	(21 tow. 000) [305/25N]			slicks trend 289 [06/199]
	110	"	35+	(67 tow. 180) [073/68S]		sense not discern.	" 280 [45/100]
3	130-134	"	46+ seems TRUE				burrows & bioturb.
	139	"	21+	(17 tow. 000) [321/26E]			difficult to match displaced burrows across fault
							slicks trend 285 [15/105]
0-150 struc. contin.	5	FAULT	22 –	(05 tow. 000) [351/30E]			slicks trend 022 [16/022]
	25-31	BRECC./GOUGE			PMAG OVERLEAF		narrow, ~6cm, zone of finely brecciated material, approx horiz. sharply bounded, presumably tectonic.
4	41	BEDDING	06–	(03 tow. 180) [153/07W]			
	90	FAULT	36–	(02 tow. 000) [183/36W]			slicks trend 037 [23/217]

— SECTION 4, 5, 6 CONTINUED ON SECOND SHEET —

Possible identifiers include : (planar structures) bedding; scaly fabric; faults; joints, shear/deformation bands; veins; pseudo-veins; fissility; fractures; fold axial surfaces; (linear structures) slickenlines; fibres; fold axes. Modifiers include : discrete; diffuse; planar/parallel; conjugate; trapezoidal; anastomosing; bifurcating; sinuous.

Figure 10. Example of the working core description sheet found useful for recording structural features. The original form measures 40 cm x 28 cm, occupying two joined U.S. letter-size sheets.

ODP LEG 131

STRUCTURAL DATA HOLE : 808C CORE 38R

DEPTH AT THE TOP : 654.9 m

HOLE OFF VERTICAL ANGLE : DIP DIRECTION

sect.	loc. cm	range cm	IDENTIFIER	working AZIMUTH	app. DIP		aux PLANE work. Az	aux PLANE Dip	app.DIP in aux.	working TREND	fault sense	fault DISPL.	THICKN. cm	SPACING cm	Magn. NORTH	orientn. method	real STRIKE	real TREND	uncor DIP	DIP dir	TRUE DIP	DIP dir	uncor plunge	TRUE plunge	apparent DEPTH m	real DEPTH m
1	3	2	bedding	180	-5										135	Pmag	45		5	E					654.93	
1	28	2	fault	121	-21	A	0	90	-33	270					135	Pmag	346	135	37	E			21		655.18	
1	47	2	fault	136	-23	A	0	90	-22	267					135	Pmag	1	132	30	E			25		655.37	
1	67	4	shear band	0	47										135	Pmag	225		47	W					655.57	
1	67	4	fault	252						33	N				135	Pmag	117	258	73	N			64		655.57	
1	73	2	fault	143	-13	A	0	90	-10	255					135	Pmag	8	120	16	E			16		655.63	
1	82	2	bedding	247	-3	A	0	90	7						135	Pmag	112		8	S					655.72	
1	82	2	fault	63	61	A	0	90	-74		N	0.2			135	Pmag	288		76	N					655.72	
1	99	2	shear band	0	0										135	Pmag	225		0						655.89	
2	0	2	fault	7	84	A					N	0.2							84	E					656.4	
2	30	2	bedding	189	-8										140	Pmag	49		8	S					656.7	
2	40	15	fault	338	62	A	0	90	37	108	N				140	Pmag	198	328	64	W			58		656.8	
2	40	15	fault	341	66	A	0	90	38						140	Pmag	201		67	W					656.8	
2	74	2	fault	149	-73	A	0	90	-63	239	N	0.8			140	Pmag	9	99	75	E			75		657.14	
2	74	2	fault	148	-62	A	0	90	-50	238	N	0.2			140	Pmag	8	98	66	E			66		657.14	
2	76	5	fault	162	-70	A	0	90	-42	252	N	0.3			140	Pmag	22	112	71	E			71		657.16	
2	76	5	bedding	180	-5										140	Pmag	40		5	E					657.16	
2	82	2	fault	320	22	A	0	90	19	90					140	Pmag	180	310	28	W			22		657.22	
2	82	2	fault	6	27	A	0	90	-3	90					140	Pmag	226	310	27	W			27		657.22	
2	96	9	fault	151	-75	A				241	N				140	Pmag	11	101	77	W			77		657.36	
2	122	2	fault	63	18	A	0	90	-33	103					140	Pmag	283	323	36	N			24		657.62	
3	20	2	bedding	247	-3	A	0	90	7						130	Pmag	117		8	S					658.1	
3	87	2	fault	305	15	A	0	90	21	109					130	Pmag	175	339	25	W			6		658.77	
3	110	3	fault	73	35	A	0	90	-67	100	R				130	Pmag	303	330	68	N			45		659	
3	139	2	fault	321	21	A	0	90	17	105	Sprob				130	Pmag	191	335	26	W			15		659.29	
3	139	2	fault	12	36	A	0	90	-9	100					130	Pmag	242	330	37	N			36		659.29	
3	140	10	fault	168	-42	A				250	R				130	Pmag	38	120	43	W			42		659.3	
3	140	10	fault	186	-38	A				260	R				130	Pmag	56	130	38	W			37		659.3	
3	140	10	fault	180	-20	A				237	R				130	Pmag	50	107	20	W			20		659.3	
4	0	4	fault	175	-40	A				264	Rprob				135	Pmag	40	129	40	W			40		659.4	
4	5	2	fault	351	30	A	0	90	5	22					135	Pmag	216	247	30	W			16		659.45	
4	41	2	bedding	153	-6	A	0	90	-3						135	Pmag	18		7	E					659.81	
4	90	2	fault	183	-36	A	0	90	2	217	R	1			135	Pmag	48	82	36	S			23		660.3	
4	90	10	shear band	35	51	A					R	0.5			135	Pmag	260		56	N					660.3	
4	94	6	fault	156	-72	A				167	S				135	Pmag	21	32	72	W			34		660.34	
5	8	2	bedding	117	-3	A	0	90	-6						230	Pmag	247		7	N					660.98	
5	15	2	fault	131	-22	A	0	90	-25	304					230	Pmag	261	74	32	N			4		661.05	
5	36	2	fault	170	-49	A	0	90	-12	323	Dprob				230	Pmag	300	93	49	N			28		661.26	
5	98	2	fault	180	-28		180	90	15	188					145	Pmag	35	43	33	W			20		661.88	
5	101	2	fault	180	-10					205	Nprob				145	Pmag	35	60	10	E			3		661.91	
5	101	2	fault	284	5	A	0	90	20	319					145	Pmag	139	174	21	W			14		661.91	
5	103	2	fault	154	-57	A	0	90	-37	206					145	Pmag	9	61	60	E			53		661.93	
5	109	16	fault	199	-75	A	0	90	-52	209					145	Pmag	54	64	76	S			34		661.99	
5	130	2	fault	82	10	A	0	90	-53	270					145	Pmag	297	125	53	N			2		662.2	
5	130	2	fault	180	-8	A	0	90		260					145	Pmag	35	115	8	E			4		662.2	
5	142	2	fault	153	-4		180	90	2	255					145	Pmag	8	110	4	W			42		662.32	
5	142	2	fault	180	-42					265	N				145	Pmag	35	120	42	W			10		662.32	
5	144	2	fault	28	15	A	180	90	8	65	Nprob				145	Pmag	243	280	17	E			10		662.34	
5	148	2	fault	281	3	A	0	90	15	82					145	Pmag	136	297	15	N			5		662.38	
6	69	2	bedding	90	0	A	0	90	-2						180	Pmag	270		2	N					663.09	
6	100	5	pseudoveins		70	A								0.4	180	Pmag									663.4	

Figure 11. Example of the spreadsheet devised for the computer storage and manipulation of structural data derived from the core descriptions. The original measures 25 cm x 17 cm and occupies a U.S. letter-size sheet. The example includes the data shown in Figure 10.

incorporate a greater degree of manipulation of the data by the computer. The description form has few, broad columns to allow the working space that was found useful while handling the cores, whereas the spreadsheet has rigorously defined columns that prompted consistent and quantitative recording of the data. The following sections are largely an explanation of these documents, because they provide a summary of the procedures used as well as insights into the difficulties and constraints encountered when dealing with structures observed only in cores.

A Simple Device for Measuring Structures

Our measurements of the orientations of structures observed in the cores were greatly facilitated by a simple tool suggested by Neil Lundberg, who drew on his experience from DSDP Leg 87. Although exceedingly simple in concept and fabrication, the device enables measurements to be made much more conveniently, rapidly, and accurately than would be possible with a protractor or a standard field clinometer.

The device is illustrated in Figure 12A. It consists, in principle, simply of a protractor-like graduated scale, with a pivoted measuring arm. More elaborate versions could be evolved according to personal preference. During measurement, one half of the arm is aligned closely against the structure of interest and the other half points to the value of the dip angle on the graduated scale.

Figure 12B shows the device being used to measure the apparent dip angle of a structure on a split core-face, a very common application. Dip angles refer, by definition, to inclinations from the horizontal, but there is no horizontal datum on a core; rather it is the vertical axis, the length of the core, that forms the obvious datum. The baseline of the clinometer is therefore aligned vertically (a procedure that requires some judgement if the core material has moved within the liner or has fragmented). With the device in this alignment, the arrangement of the graduated scale is such that when the measuring arm is rotated from horizontal to vertical the readings increase from 0° to 90°. *Note that this is the opposite arrangement from that found on a conventional protractor.* The device as suggested here therefore reads the dip angles directly, eliminating the mental arithmetic necessary if it is constructed from an ordinary protractor.

The multiple baselines of the device illustrated here allow some choice of where the tool is positioned against the core edge, so that the measuring arm can be closely aligned with the structure being measured. The tool is therefore best made of clear plastic, although the measuring scale would be easier to read if it were dark on a white background. The arm design suggested here requires that it is transparent. The pivot on the underside of the clinometer should be as nearly flush as possible, so that the instrument can fit close to the core face.

The advantages of the tool apply equally to measuring a dip angle at right-angles to the core-face (Fig. 12C), or on some surface along which the core has broken. Such additional dip readings are commonly needed to help establish the true-dip value of a structure. Note that in the device illustrated here the half of the measuring arm that is aligned with the structures has been made relatively short, about 3 cm, so that it could be held against fracture surfaces without having to remove the material from the core liner.

A further application of the tool is the measuring of azimuths. Figure 12D shows the base line of the device aligned parallel with the split core-face, and the arm being used to measure an azimuth. The arrangement of the scale is correct for the azimuthal reference frame used on Leg 131 (see next section), where 000 or "pseudo-north" is at right-angles to the core-face of the archive half of the split core, provided the azimuths fall in the "northeast" quadrant; those falling in the "northwest" quadrant will require the reading to be subtracted from 360°.

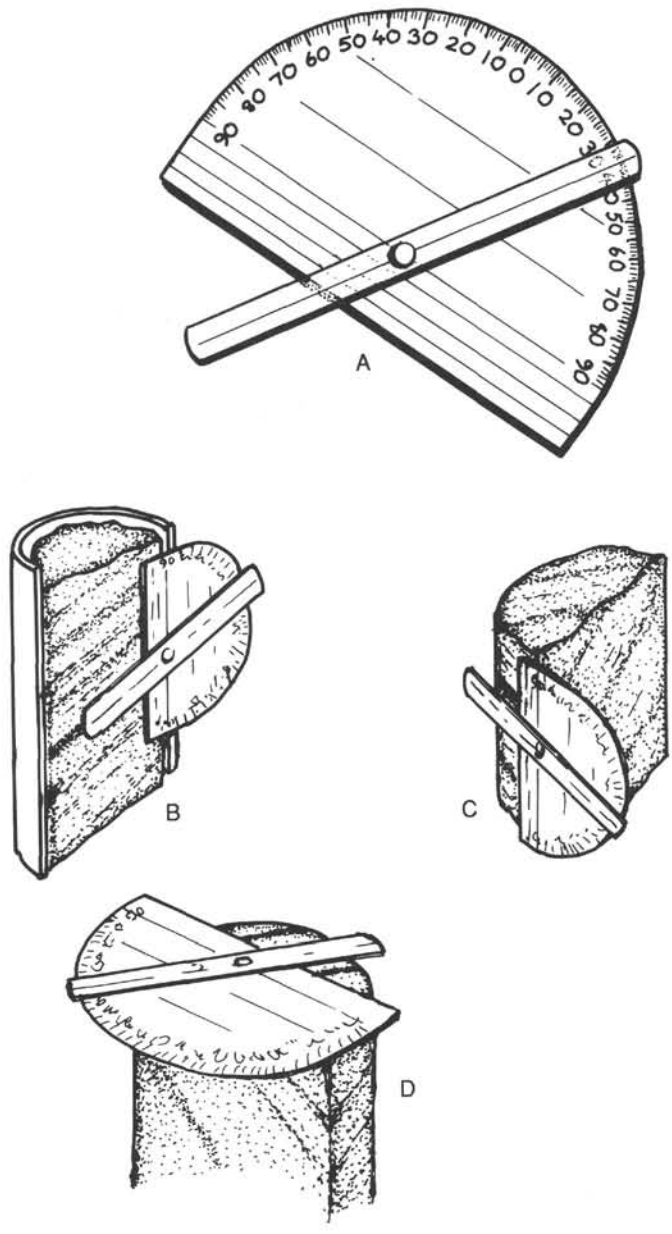

Figure 12. **A.** Drawing of a device for measurement of core-structure orientations. **B.** Device being used to measure the dip of a structure on the face of a split core. **C.** Device being used to assess the dip of a structure as seen at right-angles to the split-core face. **D.** Measuring the azimuth of a structure as seen on an upper surface of a core.

In the Site 808 chapter (this volume) we discuss the kinds of structural geological measurements of cores that were made on Leg 131. However, the device also found application in measuring the orientations of bioturbation marks and paleocurrent indicators. All of these operations are greatly facilitated by having available the kind of device described here.

Description of the Structures

A fundamental aspect of the core description was the recording of the orientations of the structures. However, relating orientations as seen in the cores to their actual subsurface disposition has long been a major problem, and

this continued to be a difficulty on Leg 131. Endeavors to deduce the real orientation of structures required two stages; first, structures were oriented relative to some "local" reference coordinates, and second, this arbitrary reference frame was related to true north and true vertical. In general, the first stage can be done routinely, although it does require collecting and converting a large number of apparent measurements. The system we used for these conversions is outlined below. The second stage depends on the availability of multishot, paleomagnetic, or formation microscanner (FMS) data. On Leg 131, correction of the data to true coordinates relied heavily on paleomagnetic information.

The descriptions and measurements of structures were based on the face of the archive half of the split core, though frequent recourse was made to the working half for additional information. The location of a structure was recorded in centimeters from the top of the section, according to conventional ODP procedure. Where a structure extended over an interval, the locations of the top and bottom of its range were recorded.

In an attempt to achieve consistency of nomenclature, the structural geologists agreed on a working descriptive terminology for macroscopic features, listed at the foot of the description form (Fig. 10). There is no implication that these features fall into distinct pigeon-holes–there is clearly some gradation and even overlap–but these aspects were brought out by adding modifiers, descriptive comments, and sketches. The description form allowed the recording of subtle variations in macroscopic appearance, but within a defined framework. The terminology was evolved from the experience of workers on previous legs. A particular problem was the naming of the structures referred to here as "shear bands" and "faults." These features almost certainly overlap with structures described previously as deformation bands, kink bands, and shear zones, but their exact nature and origin will remain unclear until shore-based studies are completed. The two terms are therefore used loosely here, for descriptive convenience rather than to imply a specific genesis.

A continuing difficulty was the distinction between natural structures and those due to coring disturbance. Planar structures with polished surfaces and/or linear grooves were regarded as tectonic rather than drilling-induced, but zones of brecciation and gouge posed a problem. Features were not recorded if a tectonic origin was in doubt. In general, the recommendations of Lundberg and Moore (1986, p. 42–43) were followed.

The dip of all structures exposed in the split cores was recorded according to the convention shown in Figure 13, that is, a two-digit angle between 00° and 90°, positive for dips to the right and negative for dips to the left, as the observer views the face of the archive half of the core, with its top upward. The dip values were recorded numerically rather than by symbols. These values were entered as an "apparent dip." Note that dips recorded at this stage assume that the long axis of the core is vertical, that is, deviations of the drill-hole from vertical are ignored.

Attempts were normally made to establish the true dip of the structures. Typically, a second apparent dip was measured in a vertical plane at right-angles to the core face (termed "auxiliary plane working azimuth" and "auxiliary plane dip" on the spreadsheet) with the apparent dip direction in this plane being either toward 000 (+ on the spreadsheet) or 180 (- on the spreadsheet). These measurements are relatively straightforward for planar structures that are at least partially visible in the sides of the core. For structures not exposed three-dimensionally in the archive half, the corresponding part of the structure could be located on the working half of the core, and a saw cut made at right-angles to the main core face. Commonly, however,

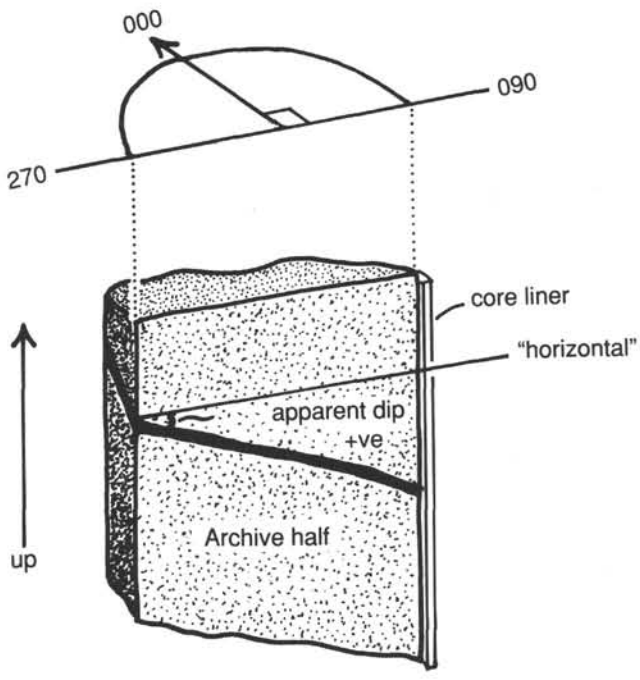

Figure 13. Diagram of the conventions used for measuring azimuths and dips of structural features seen on the face of the split core.

this was unnecessary as a broken surface in the core allowed the structure to be measured in a plane other than the core face. In this case the orientation of the fracture surface was recorded as "auxiliary plane working azimuth" and "auxiliary plane dip." The orientation of the structure, as seen on the core sides, fracture, or sawn surface, was entered on the spreadsheet as "apparent dip in auxiliary plane."

At the time, it was found more efficient to derive the true dips stereographically on a computer than to rely on spreadsheet manipulations. Future improvements to the spreadsheet should allow such conversions to be made directly and dependably on the spreadsheet. We used the Stereonet Plotting Program of R. W. Allmendinger, Version 4.1-11, on an Apple-Mac PC. The two apparent dip orientations were entered as lines, and the computer found the great circle of cylindrical best fit to both lines. The orientation of this great circle gave the "working azimuth" and "true dip" of the observed structure, which was recorded on the description form in square brackets and also entered into the spreadsheet. Where a structure was seen as a three-dimensional plane in a fragmented piece of core, or its trace could be observed at the top or bottom of a core section, it was possible to measure directly the true dip and working azimuth.

The latter measurement is, of course, equivalent to the strike of the structure, but because at this stage the orientation of the core with respect to north is not known, the azimuth has to be referred to some arbitrary reference frame. The convention shown in Figure 13 was adopted, where 000 (a "pseudo-north") is the direction that leaves the archive half at right-angles and goes from the exposed face to the single line on the core liner. Because the structural descriptions are based on the archive half of the core, it was found more convenient to define the reference frame with respect to that half rather than the working half as is used in some other conventions.

Azimuths falling in the northeast quadrant were recorded as three-figure values between 000° and 090°; those in the northwest quadrant were given values between 270° and 359°. Where an azimuth was derived by measuring the working half

of the core, care had to be taken to refer the values back to the archive-half reference frame.

At the top and bottom of the core and on broken pieces, it was occasionally possible to discern linear structures such as the hairline grooves associated with faults and shear bands, called here slickenlines. The orientations of these and all other lineations were recorded as a "working trend," measured in the direction of plunge and referred to the local 000° in the same way as planar surfaces.

The sense of fault displacement was also routinely recorded, as it appeared on the core-face or on the tops of broken pieces. Displacements seen on the core-face were treated as dip-slip, and referred to as normal or reverse movements; those observed on top faces were regarded as strike-slip and termed sinistral or dextral. Clearly, these are apparent motions, and only by combining them with displacements seen on a cut surface in the working half or observing slickenline orientations was it possible to resolve between dip-, strike-, and oblique-slip. Similarly, the magnitudes of displacement were routinely measured on core-faces and tops, giving apparent values only. The measurements were normally made parallel to the fault trace, as straight-line separations between displaced planar markers. In some cases, several cuts were made to constrain better the true displacement values of the faults.

Real Orientation of the Structures

Following the recording of orientation data on the descriptive sheets as outlined above, it was necessary to convert these local orientations to real geographical coordinates. The multishot technique allows piston cores to be oriented with respect to magnetic north, and hence the arbitrary local reference frame to be positioned, but on Leg 131 the technique was found to be highly unreliable. Consequently, the paleomagnetic approach was routinely employed and, provided the core material was reasonably consolidated, found to be very successful. It was especially useful for cores obtained by Rotary and Extended Core Barrel drilling because these techniques often caused the core to break into several pieces that rotated independently of each other within the core liner. To remove these drilling-induced rotations, paleomagnetic information was gathered from sections of core that were considered to be structurally continuous, that is, rotated as a single piece. The magnetic data, obtained by the cryogenic magnetometer from the demagnetized archive halves of the cores, are routinely collected and stored in the paleomagnetic lab. With the aid of the onboard paleomagnetic specialists, we found it possible to apply this information to the structural measurements. To obtain the data from samples shorter than the averaging limits of the cryogenic magnetometer – typically this would apply to pieces less than 10 cm in length – the individual pieces were removed from the working half of the core and run through the instrument without demagnetization. Both methods provided the declination and inclination of the natural remanent magnetism in the sample, which could then be used for orienting the structures.

The spreadsheet allows for "uncorrected dip" to be converted to "true dip," that is, to allow for movement of the material within the core-liner and for deviations of the drill-hole from vertical. On Leg 131, however, the paleomagnetic inclinations were found to be too imprecise to make these corrections. Also, the multishot device failed to produce directions for any drift of the drill hole, so this means of correction was also impracticable. However, the instrument did indicate that deviations from vertical were consistently less than 3° and hence could be neglected.

Knowledge of the magnetic declinations was highly useful. Paleomagnetic convention employs a "pseudo-north" or 000° direction in the working half of the core, and so the first step was to adjust the magnetic declination by 180° so that it corresponded with our reference frame based on the archive half. The adjusted declination was recorded as "magnetic north" on the spreadsheet. As with the apparent dip to true dip corrections mentioned earlier, we had insufficient time while aboard ship to develop the spreadsheet program so that it could handle all the possible spatial configurations of rotating planes and their associated changes of dip direction, and so individual working azimuths had to be rotated stereographically on the computer. This did have the advantage of allowing a visual check and direct printing of the corrected data, although the spreadsheet could be developed to make the corrections directly. By adding or subtracting, as appropriate, the difference between the 000° reference direction and magnetic north, the core measurements were rotated to a geographically correct orientation. The steps are summarized in Table 6. Having made this correction, the new azimuths were referred to as "real strikes" and "real trends." The procedures are intricate and time-consuming, but they have led, for the first time on an ODP leg, to a comprehensive inventory of deformation structures throughout the cores together with their real geographic orientations.

True Position of the Structures

The "apparent depths" on the spreadsheet are the values as they appear in the core according to normal ODP convention; "real depth" refers to the actual depth in meters below seafloor (mbsf). This adjustment depends on the availablity of FMS data, and in any case is only possible in a reconnaissance way while we are aboard ship; conversion to reliable depth profiles requires complex processing that at present cannot be carried out during a leg.

The various corrections to orientations and positions that were possible aboard ship have led to the structural syntheses presented in the site descriptions. Some of the interpretations will be refined after further work because in addition to describing the cores, the structural geologists collected sam-

Table 6. A summary of the steps involved in converting measurements of structures observed in split cores to real geographic coordinates.

1. Identify features and measure apparent dips on archive-half of core.
2. Look for auxiliary surfaces that provide further orientation information.
3. If necessary, refer to working-half of core for auxiliary information. (Refer azimuths to 000 "pseudo-north" in the archive half.)
4. Derive true dip and azimuth orientations (e.g., using Stereonet Plotting Program of R. W. Allmendinger, plot apparent dip directions and angles as lines, and find cylindrical best fit.)
5. Correct dip angles for deviation of drill hole from vertical, if this information is available.
6. Select representative piece from continuously oriented part of core and pass through the cryogenic magnetometer. If the core section underwent little differential rotation during drilling, it may be reasonable to average the entire section. Derive the magnetic declination.
7. Adjust the magnetic declination by 180° (The paleomagnetic 000 reference point is located in the working half, 180° away from the reference point used in structural measurements.) The adjustment is unnecessary if the magnetic declination of the working-half was measured.
8. If the adjusted paleomagnetic declination falls between 000 and 180°, subtract its value from the working azimuths to obtain the real strike, adjusting the dip direction as appropriate. If the adjusted paleomagnetic declination falls between 180° and 359°, add its value to the working azimuths, and adjust dip directions. These operations are conveniently carried out stereographically (by rotating the orientations of the planes around a vertical axis by the required amount and in the appropriate direction), which allows both visual checking of the manipulation and direct printing of the results.
9. Record paleomagnetically corrected real strike and true dip.

ples for shore-based analysis. An array of instrumental and analytical techniques will explore the nature of the structures in detail, and attempt to quantify the various stress and strain tensors. The emphasis while we were aboard ship was on thorough and careful description of the range of structures observed.

PALEOMAGNETICS

Paleomagnetic studies on Leg 131 involved the measurement of natural remanent magnetization (NRM), and remanence after progressive alternating field (AF) demagnetization. Measurements were made on continuous sections of the archive half-core and on selected discrete samples. Alternating fields of up to 15 mT were applied to material from the archive half of the core; higher fields were used, where appropriate, on samples taken from the working half. Where there was evidence of a primary remanence, its inclination was used to assign a magnetic polarity to the sediment column. The magnetostratigraphy thus erected was dated by reference to Berggren et al. (1985).

Beyond this primary application of paleomagnetism, extensive use of remanence measurements was made by structural geologists and sedimentologists, to provide directional control for their observations.

Magnetic susceptibility of the core sections was measured as part of the physical properties package (see Physical Properties section, this chapter).

Instruments

Magnetic remanence measurements on continuous sections of core were made with the shipboard 2-G Enterprises (Model 760R) three-component, pass-through cryogenic magnetometer. This is integrated with an online, static AF demagnetizer, which applies fields sequentially along three orthogonal axes. The magnetometer, the AF demagnetization system, and the core drive system were linked through a FASTCOM4 multiserial communications board in an IBM PC-AT-compatible computer. Measurements were controlled by a modified version of a University of Rhode Island BASIC program.

It is useful to examine carefully the interpretation, in terms of (relative) declination, inclination, and intensity, of the three-component output from the cryogenic magnetometer. The magnetometer sensors are designed primarily to provide a region of uniform response, at their common center, for discrete-sample measurement. The response of each sensor is geometry-dependent and slightly different: in particular, the response for the Z sensor (with coil axis along the core-transport axis) is a symmetrical positive peak, while for the X and Y sensors (with coil axes perpendicular to the core-transport direction) the response is a central positive peak, flanked by subsidiary negative wings. In the absence of an algorithm to invert continuous-core measurements, the interpretation algorithm presently employed is based on an assumption of uniformly magnetized core. In cases where the core is not uniformly magnetized, either through natural processes or artifacts (the presence of gaps in the core, or differential rotation of segments within the core-liner), the values of declination, inclination, and intensity should be treated with caution. The last case mentioned, of relative rotation of segments, occurs most frequently in practice. Its effects are illustrated in Figure 14. In simple terms, across a rotated break between segments of uniform magnetization, the Z component (and hence the polarity) will be unaffected, but the resultant X and Y components will be underestimated, resulting in a smooth variation in apparent declination, an increase in the magnitude of apparent inclination, and a decrease in apparent intensity across the break (Fig. 14A). In, for example, "biscuited" material, where the core consists of many short fragments, the resulting pattern is of very scattered declinations and steep inclinations (Fig. 14B). Only where measurements are consistent across an interval larger than the sensing region of the magnetometer can reliable declination and inclination values be inferred (Fig. 14C).

A further potential source of error in using the cryogenic magnetometer was identified. It is associated with the positioning of samples in the magnetometer for measurement. For a sample placed at the mutual center of the pairs of sensor coils, each pair senses only the component of magnetization parallel to the axis of those coils. However, if the specimen is displaced from this position, orthogonal components of magnetization may produce unbalanced responses in the two coils of a pair, leading to a net "cross-talk," not at present accounted for in the data analysis routines. In practice, in measuring half-cores, a misplacement vertically is the most likely error: care should be taken to mount samples as close to the center line as possible.

Discrete samples were measured either using the cryogenic magnetometer programmed in discrete mode, in which case short segments of core could be measured directly, or using a Molspin Minispin spinner fluxgate magnetometer, for which cubical or cylindrical samples, depending on lithology, were taken from the working half of the core. Cylindrical "minicores" were preferred; to preserve orthogonality in orientation, these were drilled, on a bench press, from sections of the working half inverted to rest on their flat upper surfaces. Some samples measured in the spinner magnetometer were demagnetized in a single-axis demagnetizer, but this line was not pursued when it was realized that a significant anhysteretic remanence was being imparted to the samples.

Subsequently, measurements were made onshore using a Digico spinner fluxgate magnetometer and a Highmoor alternating field demagnetizer, which incorporates a two-axis tumbler.

INORGANIC GEOCHEMISTRY

Interstitial Water Chemistry

To a large extent the shipboard inorganic geochemistry program has focussed on the retrieval of interstitial waters by means of hydraulic press- actuated extrusion of samples obtained from whole-round cores. Special attention was given to close-spaced sampling in the upper 25 m (2 whole- round core samples for each core), followed by one sample each in each subsequent core (length 10–25 cm, depending on the nature of the core, deeper cores requiring larger sections for sufficient interstitial water recovery). In the upper part of the sediments, which was sampled by means of the hydraulic piston corer, whole-round cores were taken after examination by the MST probe for physical properties. This ensured continuity of the physical property data base. Care was taken that the end caps were not sealed with acetone prior to taking the inorganic geochemistry whole-round samples. Great care was taken to minimize the effects of core contamination by drill pipe waters through the removal of any suspicious material from the outside of the whole-core sample and along cracks and fissures.

After careful selection of the core sample, with special attention to the avoidance of contamination, samples were introduced into a titanium Manheim squeezer (courtesy of P. Froelich). In addition, use was made of stainless-steel Manheim squeezers. Samples were extracted as soon as possible after recovery, but were in essence all obtained at room temperature. As *in-situ* temperatures varied from 2°–100°C, this may lead to some artifacts (Sayles et al, 1973; Gieskes,

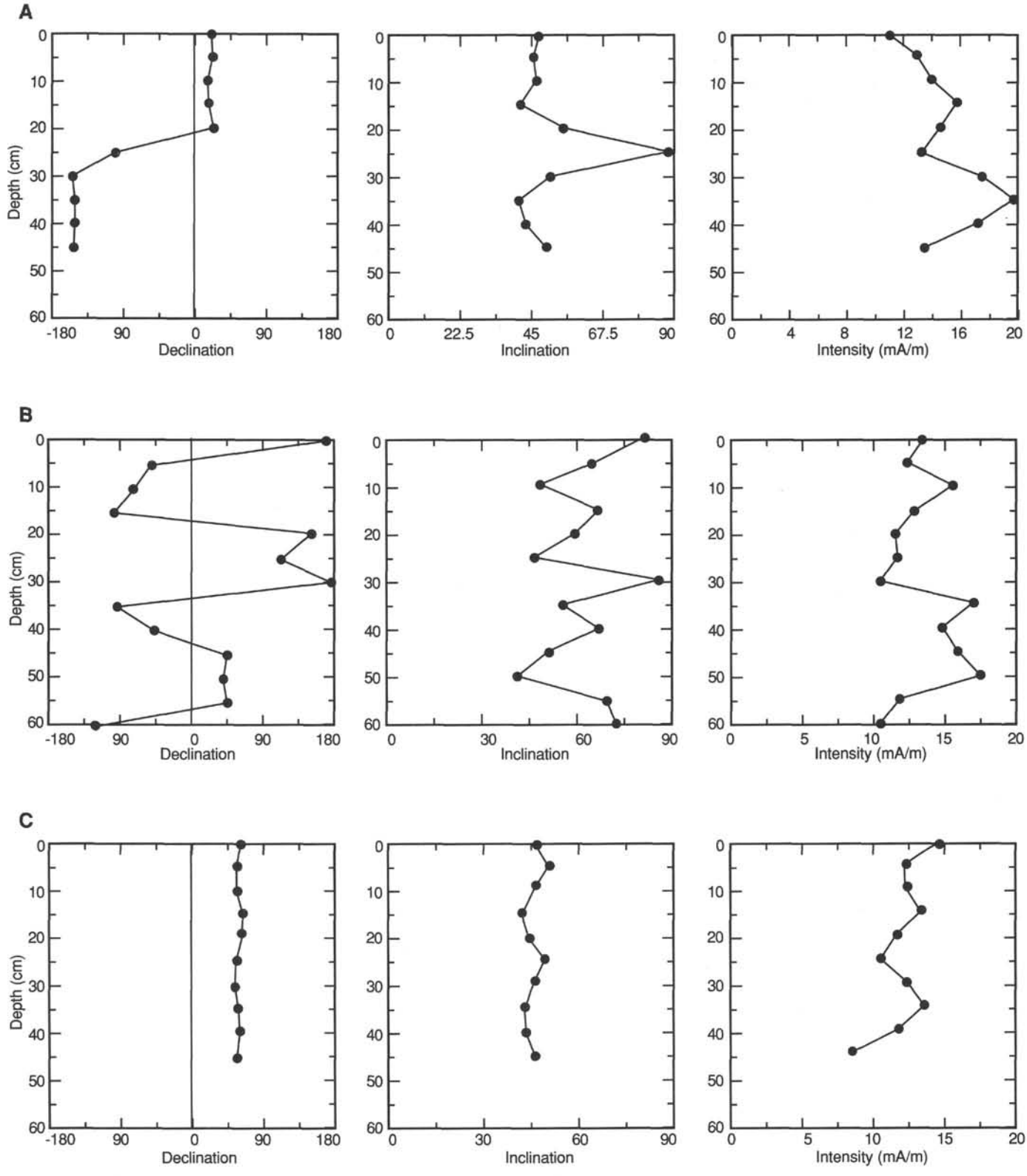

Figure 14. Declination, inclination, and intensity values interpreted from the X-, Y-, and Z-component readings of the cryogenic magnetometer. In all of the following cases the expected remanence inclination is about 50°. **A.** At a rotated break, the declination changes smoothly, the magnitude of the inclination peaks and the intensity drops slightly. **B.** Over many, short, rotated segments the magnitude of the inclination is biased to high values. **C.** Where the core is uniformly magnetized over an interval exceeding the response distance of the sensors, reliable values are obtained.

1973, 1974), but overall trends will not be obscured and especially concentration variations in nearby cores will not be obscured. All samples were filtered through 0.45-μm Gelman acrodisc disposable filters and subsequently subdivided for both shipboard work as well as for future work in shore laboratories.

Additional samples were recovered from the WSTP sampler whenever this instrument was deployed.

Shipboard analyses included:

Salinity	Goldberg refractometer
pH, Alkalinity	Automatic titration
Calcium	EGTA titration
Magnesium	EDTA titration (corrected for calcium)
Chloride	Mohr titration
Sulfate	DIONEX ion chromatography
Ammonia	Colorimetry
Phosphate	Colorimetry
Silica	Colorimetry
Potassium	Atomic emission spectrometry
Lithium	Atomic emission spectrometry
Sodium	Atomic emission spectrometry
Strontium	Atomic emission spectrometry

Procedures for the above analyses are described by Gieskes and Peretsman (1986) and Atomic emission spectrometry procedures were based on a modification of the methodology developed by Hans Brümsack (pers. comm., 1990) during Leg 127. During Leg 131 these methods were consolidated into a new version of the chemistry cookbook (Gieskes, Gamo, and Brumsack, in press).

Solid Phase Chemistry

Shipboard carbonate carbon and organic carbon/nitrogen analyses were carried out on a routine basis on samples provided by the core laboratory as well as on samples collected in the chemistry laboratory. Carbonate analyses were carried out by coulometric analysis. Organic carbon/nitrogen analysis was carried out by means of a Carlo Erba C/N analyzer.

Solids obtained from interstitial water (IW) samples were analyzed for their bulk mineralogy by X-Ray diffraction. Ash samples were analyzed by wet chemical techniques (Donnelly, 1980), using methodologies consolidated into a new shipboard cookbook (Gieskes and Gamo, in press).

Pressure Core Sampler

During Leg 131 a new version of the pressure core barrel was tested. This apparatus was designed specifically for the retrieval, under *in-situ* conditions, of a core in the zones of clathrate occurrences. Upon retrieval interstitial fluids are expelled either by means of a gas displacement technique or the core is immediately frozen in liquid nitrogen for transport to the shore laboratory, where the sample will be retrieved under *in-situ* pressure and temperature. This apparatus will play an important future role in the study of gas hydrate-containing sediments, not only with respect to the chemical properties, but also with respect to the physical properties of these sediments.

ORGANIC GEOCHEMISTRY

Shipboard organic geochemistry during Leg 131 was conducted to supply a real-time monitoring of volatile hydrocarbons for safety considerations and for an initial characterization of the content and type of gases and sedimentary organic matter. These analyses provide a basis for the preliminary Site Summaries and background for the more detailed shore-based studies.

Elemental Analyses

Sediments were analyzed on board ship for inorganic carbon and for total nitrogen, carbon, and sulfur. The total organic carbon (TOC) content of the sediments was then calculated by subtraction of the inorganic carbon content from the total carbon content. The analyses were carried out on sediment residues from headspace gas analyses, the sediments being freeze-dried prior to analysis.

Total inorganic carbon was determined using a Coulometrics 5011 coulometer equipped with a System 140 carbonate carbon analyzer. Depending on carbonate content, 15 to 70 mg of ground and weighed sediment was reacted in a 2N HCL solution. The liberated CO_2 was titrated in a monoethanolamine solution with a color indicator, while the change in light transmittance was monitored with a photodetector cell.

Total nitrogen, carbon, and sulfur were determined using a NA 1500 Carlo Erba NCS analyzer. Bulk samples were combusted at 1000°C in an oxygen atmosphere with addition of vanadium pentoxide, converting organic and inorganic carbon into CO_2 and sulfur to SO_2. These gases along with nitrogen were then separated by gas chromatography and measured with a thermal conductivity detector (TCD).

Gas Analyses

Gases were extracted from bulk sediments utilizing headspace sampling techniques (Emeis and Kvenvolden, 1986). A 5-cm^3 plug of sediment was taken as the core arrived on deck, utilizing a No. 4 cork borer. The sample was placed immediately in a glass vial that subsequently was sealed with a septum and metal crimp and then heated to 70°C and kept at this temperature for 45 min.

Gas pocket samples were obtained by expanding gases from visual pockets into pre-evacuated and sealed glass tubes (Vacutainers). For this purpose one end of an injection needle is inserted through the rubber stopper of the Vacutainer and the other end through the plastic liner into the gas pocket.

All headspace gas and Vacutainer samples were expanded into a gas-tight syringe and injected into an HP 5890A NGA gas chromatograph for flame ionization detector (FID) and thermal conductivity detector (TCD) analyses. The gas chromatographic system employs a 6-in. x 1/8-in. steel column packed with Poropak T, a 3-ft x 1/8-in. steel column with a 13× molecular sieve, a 6-ft x 1/8-in. steel column packed with 80/100 mesh Hayesep R(AW), and a DB1 (1-mm film thickness, J&W). Appropriate automatic valve switching, controlled by an HP 3392 Integrator that also recorded and integrated the count rates, provided a rapid determination of oxygen, nitrogen, carbon dioxide, and hydrocarbons from methane to hexanes. The separation on the FID line was carried out isothermally at 40°C at a flow rate of 2.24 mL/min. Helium was used as carrier gas.

All gas concentrations are reported in ppm.

BASEMENT LITHOLOGY AND GEOCHEMISTRY

Core Curation and Shipboard Sampling

Igneous rocks recovered during drilling were split into archive and working halves using a rock saw with a diamond blade. The petrologist decided on the orientation of each cut so as to preserve unique features and/or expose important structures. The archive half was described and samples for shipboard and shore-based analyses were removed from the working half. Each piece is numbered sequentially from the

top of each section, beginning with the number 1. Pieces were labeled at the top on the rounded, not sawn, surface. Pieces that could be fitted together were assigned the same number, but were lettered consecutively (e.g., 1A, 1B, 1C, etc.). Spacers were placed between pieces with different numbers, but not between those with different letters and the same number. The presence of a spacer may represent a substantial interval of no recovery. Whenever the original unsplit piece was sufficently large that the top and bottom could be distinguished before removal from the core liner (i.e., the piece could not have rotated top to bottom about a horizontal axis in the liner during drilling), an arrow was added to the label pointing to the top of the section, and/or a red wax cross is marked on the base of each piece. Because pieces are free to turn about a vertical axis during drilling, azimuthal orientation is not possible.

After the core was split, the working half was sampled for shipboard physical properties, magnetics, X-ray fluorescence (XRF), and thin-section studies. These samples may take the form of minicores and, if appropriate, were stored in seawater prior to physical properties measurements. Normally samples were taken from each lithologic unit when recovery permitted. The archive half was described in the visual core description (VCD), used for nondestructive physical properties, and then photographed before storage.

Visual Core Description

Hard rocks sampled from the basement were described using a VCD form specific to igneous and metamorphic rocks (Fig. 15). The left-hand column is a graphic representation of the archive half. A horizontal line across the entire width of this column denotes a plastic spacer glued between rock pieces inside the liner. The number of each piece was also recorded. Oriented pieces are indicated on the form by an upward-pointing arrow to the right of the piece. Shipboard samples and studies were indicated in the "shipboard studies" column, using the following notation:

XF = X-ray fluorescence analysis
TS = thin-section billet

As igneous rocks are classified mainly on the basis of mineralogy and texture, a checklist of macroscopic features was followed to ensure consistent and complete description, the details of which were later stored on a computerized database (HARVI).

When we described fine-grained and medium-grained extrusive rocks and dikes, the core was subdivided into lithological units using the criteria of changing grain size, occurrence of glassy margins, and changes in petrographic type and phenocryst abundance. Table 7 summarizes the information recorded in each lithologic unit.

Thin-Section Description

Thin-section billets of basement rocks recovered were examined to: (a) confirm the identity of petrographic groups in the cores; (b) better understand the textures and interrelationships of the mineral phases; (c) help define unit boundaries indicated by hand-specimen core description; and (d) define the secondary alteration mineralogy. Percentages of individual phenocryst phases were estimated and were reported on the detailed thin section description forms. The terms "sparsely," "moderately," and "highly" phyric were used in the same manner as for hand-specimen descriptions. Petrographic descriptions together with estimates of the various mineral phases (both primary and secondary) were made on the igneous thin-section description forms, which were also entered in the VAX computer database program HRTHIN. In cases where discrepancies arose in the lithostratigraphic summary over the composition and abundance of phenocryst phases between hand-specimen and thin-section analyses, thin-section descriptions were used in preference to hand-specimen descriptions.

X-ray Fluorescence Analysis

Because the XRF spectrometer was inoperative, XRF analyses could not be done on board ship. Samples considered to be representative of individual lithologic subunits and main units were analyzed for major oxides and selected trace elements at the Istituto di Mineralogia, Ferrara University, Italy, immediately after the cruise. The XRF system utilized for analysis is a fully automated wavelength-dispersive Philips PW1400 spectrometer, using a 3-kV Cr X-ray tube as excitation source for major elements and a 3-kV W X-ray tube for trace elements. A list of analyzed elements and operating conditions is given in Table 8.

Sample preparation involves: (a) crushing the sample to a powder and (b) production of pressed powder pellets for both majors and traces. Initially, about 5–10 cm^3 of rock were removed from the core to make the thin section: the same piece was utilized for the XRF analyses. Unwanted veins were removed using a diamond blade microtome; part of the veins were stored for successive XRD analyses. Each sample was then ultrasonically washed in distilled water for 10 min and dried at 100°C for 2 hr. Pieces were reduced in size by crushing in a hydraulic press. Powders were produced by grinding pieces in agate mortar and pestle to minimize contamination. About 0.2 cm^3 of polyvinyl alcohol was added to about 5 g of rock powder. This mixture was then pressed into a stainless-steel cylinder with about 4 tons of pressure.

Major elements are determined on pressed powder disk supported by boric acid mixed with wax. Full matrix corrections are made following the method of Franzini et al. (1975) in which the concentration of an element i is given by:

$$C = I_i * \sum_{J=1}^{N} K_{ij} * C_j \qquad (1)$$

where:
Ci = concentration of oxide i (wt %);
I_i = net peak X-ray intensity of oxide i;
N = number of analyzed oxides;
K_{ij} = matrix correction coefficients which depend, in turn, on the absorption coefficients;
C_j = concentration of the other oxides in the rocks.

Matrix correction coefficients K_{ij} are obtained from this equation using international reference samples. The concentration is obtained after some cycles of computation where in each cycle the concentration C_i is substituted with the previously obtained concentration C_i for that element until the difference $(C_i)_m - (C_i)_{m-1}$ is less than a small prefixed value, that being the number of cycles m. Major oxide percentages are then reported to 100%, considering loss on ignition (LOI) values. LOI is obtained by heating at 1100°C for 8 hr. MgO was analyzed by the atomic absorption method. For computation of trace-element concentrations the same powder disks are used following the calculation routine of Leoni and Saitta (1976); calibration curves are derived from the measurement of well-analyzed reference rocks (e.g., BHVO 1, AGV 1, BR, DRN, G2, etc.).

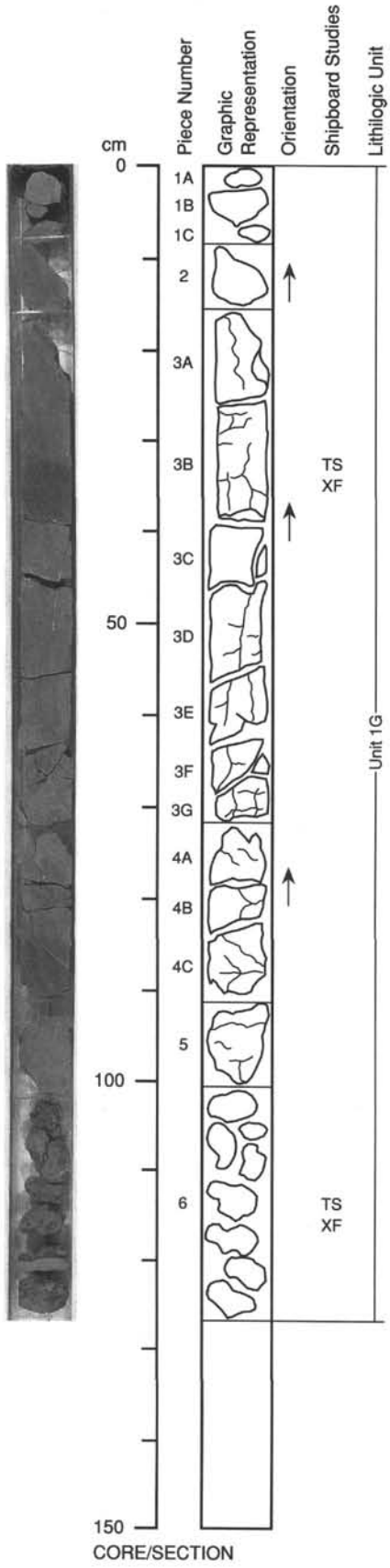

131-808C-107R-1

UNIT 1G: APHYRIC BASALT

Pieces 1-6

CONTACTS: None.
PHENOCRYSTS: Aphyric.
GROUNDMASS: Very fine grained intersertal often radiating made of 20% plagioclase laths (~0.8 mm),~25% prismatic or tabular clinopyroxene (~0.5 mm), ~5% subhedral olivine totally altered, trace of magnetite, and 10-40% interstitial partly devitrified and altered glass.
VESICLES: 0-2%; ~0.3 mm; spherical; randomly distributed; filled mainly with calcite, sometimes with spherulitic texture.
COLOR: Gray to yellowish gray with reddish haloes.
STRUCTURE: Massive.
ALTERATION: Slightly to moderately altered.
VEINS/FRACTURES: 2-10%; 0.5-3 mm; irregular;occur throughout the unit cross cutting each other: very often pieces broke along veins and commonly oxidation reddish haloes are observed on both sides of veins. One large (2-3 mm) vein crosses Pieces 3B and 3C (dip 70°) and is filled with fibrous calcite, chlorite, smectite, and Fe-oxide. Thinner veins are filled mainly with calcite or calcite and smectite and minor zeolite (?).
ADDITIONAL COMMENTS: Texture and mineral proportion are very constant along the subunit.

Figure 15. Example of a completed visual core description form for igneous rocks.

Table 7. Description, outline, and classification for fine-grained and medium-grained extrusive rocks and dikes.

A.1.	Leg, Site, hole, core number, core type, and section number.
A.2.	Unit number (consecutive downhole), rock name, the section(s) and piece number making up the complete unit.
A.3.	Contact type (e.g., intrusive, discordant, depositional, etc.) and dip, and the presence of any associated glass or its alteration products.
A.4.	The number of phenocryst phases and their distribution within the unit. For each phenocryst phase: (I) abundance; (II) average size in mm; (III) shape; (IV) the degree of alteration; and (5) further comments.
A.5.	Groundmass texture: glassy, microcrystalline, fine-grained (<1 mm), medium-grained (1–5 mm), or coarse-grained (>5 mm). Relative grain size changes within the unit (e.g., coarsening from Piece 1 to Piece 5).
A.6.	Color and variation within units. Colors are coded using the Munsell color chart (Munsell Soil Color Charts, 1971) and recorded when the core is dry.
A.7.	Vesicles: percentage abundance, distribution, size, shape, fillings, and their relationships (include proportion of vesicles that are filled by alteration minerals).
A.8.	Structure: massive flow, pillow lava, thin flow, breccia, hyaloclastite, etc., and comments.
A.9.	Alteration: fresh (<2% altn.), slightly (2%–10% altn.), moderately (10%–40% altn), highly (40%–80% altn.), very highly (80%–95% altn.) or completely (95%–100% altn.) alterated. Type, form, and distribution of alteration.
A.10.	Veins/Fractures: percent present, width, orientation, fillings and relationships. The relationship of the veins and fractures to the alteration is also noted.
A.11.	Comments: notes on the continuity of the unit within the core, and the inter-relationship of units are added here, when appropriate.
A.12.	Basalts are termed aphyric, sparsely phyric, moderately phyric, or highly phyric, depending upon the proportion of phenocrysts visible with the hand lens or binocular microscope (approximately x10). Basalts are called aphyric if phenocrysts clearly amount to less than 1% of the rock, sparsely phyric if phenocryst content ranges from 1%–2%, moderately phyric at 2%–10%, and highly phyric if phenocrysts amount to more than 10% of the rock. Basalts are further classified by phenocryst type (e.g., a moderately plagioclase-olivine phyric basalt contains 2%–10% phenocrysts, most of which are plagioclase, with lesser amounts of olivine).

PHYSICAL PROPERTIES

Introduction

General Objectives

The standard procedures for shipboard measurement of physical properties were modified and substantially expanded to serve a number of special objectives unique to ODP Leg 131. The principal objectives for the physical properties group underlie the themes of this cruise. They can be grouped together as follows:

1. Mechanical state of accreted sediments in the wedge toe;
2. Physical and deformational properties of sediments during frontal accretion; and
3. Assessment of geohydrologic conditions.

To correlate shipboard and shore-based laboratory measurements with the *in-situ* state of stress and to better constrain existing mechanical models, the specially equipped downhole tools WSTP (water sampling, temperature, and pressure measurement) and LAST-I (lateral stress tool) were employed. Measures of the amount of anelastic strain recovery (ASR) were attempted on several RCB core samples. Numerous whole-round samples from APC/XCB cored sections for onshore consolidation, permeability, and strength testing were taken during the cruise.

Standard shipboard measurements of physical properties included nondestructive, whole core, multisensor track (MST) measurements, undrained shear strength, thermal conductivity, magnetic susceptibility, electrical resistivity, compressional wave velocity, and index properties. They were performed to document the evolution of sediment physical properties during the process of frontal accretion and imbrication. Sampling frequency for most parameters was significantly increased from standard shipboard procedures to resolve and correlate properties with other shipboard data, particularly with downhole geophysical logs. On average, one sample was selected every 70 cm downhole. To characterize physical boundary conditions governing the development of structural deformation features and failure indicators, special emphasis was placed on adequate coverage of relevant areas.

Sampling Strategy

To accommodate the above-formulated general objectives, the sampling program for physical properties was planned to fulfill several requirements:

1. Provide a comprehensive record of recovered core properties. Generally, sections were scanned using the MST prior to sub-sampling for whole rounds. Samples were selected on the average of two per section.
2. Cross-correlate shipboard analyses. Samples were selected in conjunction with sedimentologists and structural geologists to identify features of interest. All physical properties analyses were made on common or adjacent sample intervals. Dried samples from index properties were forwarded to the chemistry laboratory for carbonate analyses, and splits from the dried portion of these were used for bulk X-ray diffraction (XRD) mineralogical determinations. Smear-slide descriptions and grain-size analyses were targeted for the same interval as physical properties sampling. Sediment XRD samples for shore-based investigations were selected adjacent to physical properties samples.
3. Calibrate downhole logs. Bulk density, porosity, acoustic velocity, and thermal conductivity from core samples provide identifying characteristics for log interpretation.
4. Cross-hole correlation. Magnetic susceptibility measurements on whole-round sections made continuously along the length of recovered core were carried out to enable correlation

Table 8. Leg 131 XRF analytical conditions. Major elements measured on K-alpha line using a Cr X-ray tube operating at 40 kV and 40 mA; trace elements.

Element	Detector	Collimator	Crystal	Angle	CT
Fe	F	F	LIF200	57.520	40
Mn	F	F	LIF200	62.975	100
Ti	F	F	LIF200	86.150	40
Ca	F	C	LIF200	113.235	40
K	F	C	LIF200	136.850	40
Si	F	C	PET	109.135	40
Al	F	C	PET	145.080	40
P	F	C	PET	89.465	100
Na	F	C	TAP	55.145	100
Nb	FS	F	LIF220	30.435	100
Zr	FS	F	LIF220	32.090	100
Y	FS	F	LIF220	33.890	100
Sr	FS	F	LIF220	35.845	100
Rb	FS	F	LIF200	25.560	100
Ni	FS	F	LIF220	71.295	100
Cr	FS	F	LIF220	107.160	100
V	FS	F	LIF220	123.235	200
Co	FS	F	LIF220	77.940	100
Ba	FS	F	LIF220	128.935	200
Ce	F	F	LIF220	111.740	200
La	F	F	LIF220	138.950	200

of stratigraphic horizons from adjacent holes and to correlate turbidite events between sites.

Laboratory Measurements

Index Properties

Index properties (bulk density, grain density, water content, porosity, dry density) were calculated from measurements of wet and dry weights and wet and dry volumes. Samples of approximately 15 cm^3 were taken for determination of index properties. In addition, whole-core determination of bulk density was measured on good-quality samples using the gamma-ray attenuation porosity evaluator (GRAPE) on the MST.

Sample mass was determined aboard ship to a precision of ±0.01 g using a Scitech electronic balance. The sample mass was counterbalanced by a known mass such that only mass differentials of less than 5 g were measured. Volumes were determined using a Quantachrome Penta-Pycnometer, a helium-displacement pycnometer. The Quantachrome pycnometer measures volumes to an approximate precision of ±0.02 cm^3. Sample volumes were repeated until two close measurements yielded volumes within 0.02 cm^3 of each other. A reference volume was run with each group of samples during the first several hundred tests. The standard was rotated between cells to check for systematic error. Preliminary results of this exercise suggest the pycnometer is fairly stable for a given cell inset, or sleeve. However, changing sleeves or insets offset the standard calibration by 0.1 cm^3.

The sample tare (beaker) calibrations were checked during transit to the first site. This recalibration was carried out on the basis of calculation of the densities of the beakers, using the corrected weights and volumes measured during the last leg. The ODP physical properties data base was updated with these corrected values.

Water Content

The determination of water content followed the methods of the American Society for Testing and Materials (ASTM) designation (D) 2216 (ASTM, 1989). As outlined in ASTM D2216, corrections are required for salt when measuring marine samples. In the case of Leg 131 sediments, all pore-water salinities were within 1 ppt of 35. In addition to the recommended water content calculation presented in ASTM D2216, which is the ratio of the pore-fluid mass to the dry sediment mass (% dry wt.), a calculation of the ratio of pore-fluid mass to total sample mass was also reported (% wet wt.). The equations for each water content calculation are as follows:

$$W_c(\%\ \text{dry wt.}) = (M_t - M_d)/(M_d - rM_t) \quad (2)$$

$$W_c(\%\ \text{wet wt.}) = (M_t - M_d) * (1 + r)/M_t \quad (3)$$

where:

M_t = total mass (saturated)
M_d = dry mass
r = salinity

Bulk Density

Bulk density (r) is the density of the total sample including the pore fluid, or $\rho = M_t/V_t$ where V_t is the total sample volume. The mass (M_t) was measured using the electronic balance, and the total volume was measured with the helium pycnometer. In high-porosity sediment, the bulk density was calculated directly using $\rho = M_t/V_t$.

Porosity

The porosity was calculated using:

$$\varphi = (W_c * \rho)/((1 + W_c) * \rho_w) \quad (4)$$

where:

ρ used in the equation is the directly measured bulk density
ρ_w is the density of pore fluid
W_c is the water content reported as a decimal ratio of % dry wt.

Grain Density

The grain density was calculated from the the dry mass (Scitech balance) and dry volume (pycnometer) measurements. Both mass and volume were corrected for salt as follows:

$$\rho_{grain} = (M_d - s)/(V_d - (s/\rho_{salt}))$$

where:

V_d = dry mass
s = salt correction
ρ_{salt} = density of salt (2.257 g/cm^3)

A comparison of grain density with specific gravity provides a check of the various shipboard measurements. The specific gravity (G_s) was calculated using the measured bulk density and water content as follows:

$$G_s = \rho/(\rho_w(\rho - \rho_w)) \quad (5)$$

where:

ρ_w = density of pore fluid

W_c is the water content reported as a decimal ratio of percent dry wt.

An initial review of the comparison between grain density and specific gravity revealed that the former is generally about 0.06 g/cm3 less than calculated specific gravity.

Dry Density

Dry density is the ratio of the dry mass (M_d) to the total volume. This value is typically used for calculations of mass accumulation. The dry density was calculated using the corrected water content and porosity for each measurement:

$$\rho_d = (\varphi/W_c) * \rho_w \quad (6)$$

Multisensor Track (MST)

The MST incorporates the Gamma Ray Porosity Evaluator (GRAPE), *P*-Wave Logger (PWL), and Magnetic Susceptibility devices in scans of the whole-round core sections. Individual unsplit core sections were placed horizontally on the MST, which moves the section through the three sets of sensors.

The GRAPE makes measurements of bulk density at 1-cm intervals by comparing attenuation of gamma rays through the cores with attenuation through an aluminum standard (Boyce, 1976). The GRAPE data were most reliable in APC and nonbiscuited XCB and RCB cores. In biscuited material, the GRAPE was turned off on the MST.

Bulk density was also determined for basalt samples using the GRAPE Special 2-Minute Count technique as described by Boyce (1976). The GRAPE measurements were made perpendicular to bedding on samples cut from the cores using the double-bladed saw. All counts for the samples and accompanying air (background) counts were made in duplicate and averaged. Grain density values from gravimetric measurements were used to correct the wet-bulk density determined by the GRAPE for deviation of the grain density of the sample from that of quartz. The precision estimated for this technique is ±1.5% (Boyce, 1976).

The PWL transmits a 500-kHz compressional-wave pulse through the core at a repetition rate of 1 kHz. The transmitting and receiving transducers are aligned perpendicular to the core axis. A pair of displacement transducers monitor the separation between the compressional-wave transducers; variations in the outside diameter of the liner therefore do not degrade the accuracy of the velocities. Measurements are taken at 2-cm intervals. Generally, only the APC and nonbiscuited XCB and RCB cores were measured. Weak returns with signal strengths below a threshold value of 100 were removed.

Magnetic susceptibility was measured on all sections at 3-cm intervals using the 0.1 range on the Bartington meter with an 8-cm diameter loop. The close sampling was carried out to provide another measure for between-hole correlation. The quality of these results degrades in XCB and RCB sections where the core is undersized and/or disturbed. However, the general downhole trends were used for stratigraphic correlation.

Velocimetry

Compressional-wave (*P*-wave) velocity measurements were obtained using two different systems during Leg 131, depending on the degree of lithification of the sediment. *P*-wave velocities were measured in softer sediment using a Dalhousie University/Bedford Institute of Oceanography Digital Sound Velocimeter (DSV). Velocity calculation is based on the accurate measurement of the delay time of an impulsive acoustic signal traveling between a pair of piezoelectric transducers inserted in the split sediment cores. The transducers used emit a 2-μs square wave at about 250 and 750 kHz. A dedicated microcomputer controls all functions of the velocimeter. The transmitted and received signals are digitized by a Nicolet 320 digital oscilloscope and transferred to the microcomputer for processing. The DSV software selects the first arrival and calculates sediment velocity; the full waveform is stored for later calculation of attenuation.

Two transducers were used, separated by approximately 7 cm, measuring the vertical (along the core axis) *P*-wave velocity. The transducers are firmly fixed at one end on a steel plate so that their separation does not change during velocity determinations.

Periodically, the separation was precisely evaluated by running a calibration procedure in distilled water. A value of sound velocity in distilled water is determined (based on standard equations) for the measured temperature, with the computer calculating the transducer separation using the signal travel time. At each sampling interval (usually two per section), the transducers were carefully inserted into the split section and velocity measured in both directions.

The Hamilton Frame Velocimeter was used to measure compressional-wave velocities at 500 kHz in discrete sediment samples when induration made it difficult to insert the DSV transducers without making any perturbations around them, and in lithified sediments and basement rocks when insertion became impossible. Samples were carefully cut using a double-bladed diamond saw. Sample thickness was measured directly from the velocimeter-frame lead screw through a linear resistor output to a digital multimeter. Zero travel times for the velocity transducers were estimated by linear regression of traveltime vs. distance for a series of aluminum and lucite standards. Filtered seawater was used to improve the acoustic contact between the sample and the transducers. The DSV oscilloscope and processing software was used to digitize waveforms, calculate velocities, and to store the waveforms for later attenuation calculations. Measurements were routinely made by propagating the waveform parallel to the core axis (longitudinal) and parallel to the split-core surface (horizontal or transverse). This approach then provides a measure of the acoustic anisotropy within the sediments.

Undrained Shear Strength

The undrained shear strength of the sediment was determined using the ODP motorized miniature vane shear device following the procedures of Boyce (1976). The vane rotation rate was set to 90°/min. Measurements were made only in the fine-grained, soft to very stiff units. The vane used for all measurements has a 1:1 blade ratio with a dimension of 1.27 cm.

The instrument measures the torque and strain at the vane shaft using a torque transducer and potentiometer, respectively. Output for torque and strain are recorded on a Hewlett-Packard X-Y recorder in volts. The shear strength reported is the peak strength determined from the torque vs. strain plot. In addition to the peak shear strength, the residual strength was determined from the same plot where the failure was not dominated by cracking of the sample (Pyle, 1984).

In the analyses of vane tests the assumption is made that a cylinder of sediment is uniformly sheared about the axis of the vane in an undrained condition, with cohesion as the principal contributor to shear strength. Departures from this assumption include progressive cracking within and outside of the failing specimen, uplift of the failing core cylinder, drainage of local pore pressures (i.e., the test can no longer be considered to be undrained), and stick-slip behavior.

Electrical Resistivity

Two approaches were followed to obtain electrical resistivity, expressed as formation factor, during Leg 131. Both methods utilize a common four-probe principle, though the configurations of these two vary. A small probe unit constructed by Northwest Metasystems, Inc., measures the potential drop between two platinum electrodes with a 1-mm spacing. The probe also contains a thermistor to register sediment and seawater temperature. This instrument was used only for comparative purposes in the APC section of Hole 808A.

The Wayne-Kerr Precision Component Analyzer was used to measure resistivity, following the procedures outlined in the Leg 127 Explanatory Notes (Shipboard Scientific Party, 1990). Electrical resistivity of the sediments was measured twice per section using a four-electrode configuration, which consists of four 2-mm stainless-steel rods with an electrode spacing of 13 mm. A 10-kHz square-wave current is applied to the outer electrodes and the difference in potential between the two inner electrodes is measured. The size of the current (typically 50 mA) is measured over a resistor in the outer circuit.

The electrodes were pushed approximately 1 cm into the split-core surface after measuring the resistance of seawater in another split liner, thus avoiding geometric differences between sediment and water samples. Most measurements were

made with the probes aligned across the core diameter (horizontal or transverse). A template was used to drill guide holes for the electrode pins in harder sediments. These holes were then filled with seawater and the core surface was then dried such that the electrodes would not communicate through a surface water film. The electrodes were then inserted into the guideholes for resistance measurements.

Thermal Conductivity

The thermal conductivity of cored material was measured every 1.0–1.5 m using the needle probe method, in full-space configuration for soft sediments (von Herzen and Maxwell, 1959), and in half-space mode (Vacquier, 1985) for lithified sediment and hard-rock samples. All measurements were made after the cores had equilibrated to laboratory temperature. Data are reported in units of W/m°C, and have an estimated error of 5%–10%. All data were corrected for *in-situ* pressure and temperature, assuming a hydrostatic pressure gradient and a temperature gradient of 110 mK/m. The pressure correction was +1% for each 1800 m (Ratcliffe, 1960). The temperature correction was +1% for each +20°C change in temperature between the laboratory and *in-situ* conditions, a value intermediate between +5% suggested by Ratcliffe (1960) for a high-porosity, water-saturated sediment and a mean value of -3% derived from data reported by Clark (1966) for several hard rocks.

Soft-sediment "Full-space" Measurements

Needle probes containing a heater wire and a calibrated thermistor were inserted into the sediment through small holes drilled in the core liners before the sections were split. The probes were carefully positioned where MST data indicated a sample of uniform properties. Data were acquired using a Thermcon-85 unit interfaced to an IBM-PC-compatible microcomputer. This system allowed up to five probes to be connected and operated simultaneously. For quality control, one probe was used with a standard of known conductivity during each run.

At the beginning of each test, temperatures in the samples were monitored without applying a heater current until the background thermal drift was determined to be less than 0.04 °C/min. Once the samples were equilibrated, the heater circuit was closed and the temperature rise in the probes was recorded. Thermal conductivities were calculated from the rate of temperature rise while the heater current was flowing.

After the heater has been on for about 60 s, the needle probe response is very close to that of a line source with constant heat generation per unit length. Temperatures recorded during a time interval of 60–240 s were fitted with the least-squares technique to the appropriate equation:

$$T(t) = (q/4\pi k) * \ln(t) + L(t)$$

where k is the apparent thermal conductivity, T is temperature, t is time, and q is the heat input per unit length of wire per unit time. The term $L(t)$ describes a linear change in temperature with time and includes the background temperature drift and any linearity that results from instrumental errors and the geometrical inadequacies of the experiment. These inadequacies include the finite length of the probe and sample.

All full-space measurements were corrected for a linear offset between measured and true thermal conductivities, determined from a series of tests with standards of known conductivities (Table 9, Fig. 16).

Table 9. Measured and known thermal conductivities of full-space standards.

Standard	Known conductivity	Measured conductivity	s.d.[1]	n[2]
Fresh water[3]	0.61	0.678	0.014	24
Fused silica	1.38[4]	1.549	0.073	48
Macor ceramic	1.61[5]	1.834	0.085	144

[1] standard deviation
[2] number of measurements
[3] 3% gelatin was added to prevent convection. Known conductivity from Powell (1958).
[4] Ratcliffe (1959)
[5] Pribnow (pers. comm.)

Lithified Sediment and Hard-rock "half-space" Measurements

Half-space measurements were made on selected samples after the cores had been split, with a needle probe sandwiched between the flat surface of a test sample and that of an epoxy block, which has a relatively low conductivity (Sass et al., 1984; Vacquier, 1985). All half-space measurements were conducted in a water bath, to keep the samples saturated, improve the thermal contact between the needle and the sample, and reduce thermal drift during the tests.

The samples were sanded with 240- and 600-grit paper to smooth the contact area, and EE & G thermally conductive compound was used to improve the thermal contact. The data collection and reduction procedures for half-space tests are identical to those for full-space tests.

Through tests with standards of known conductivities, we determined correction factors, taken to be linear as a first approximation, for each of three needles in the half-space bath (Lee, 1989) (Table 10, Fig. 17). These corrections are specific to a fixed time interval of 60–240 s, and account for the imperfect nature of the experiment, i.e., epoxy is not a perfect insulator, there is never an ideal thermal contact, the thermal compound may act as a heat sink, the heat source is not positioned exactly at the boundary between the sample and epoxy.

Subsequent to Leg 131, half-space calibrations for a basalt standard were found to be about 5% higher than values used

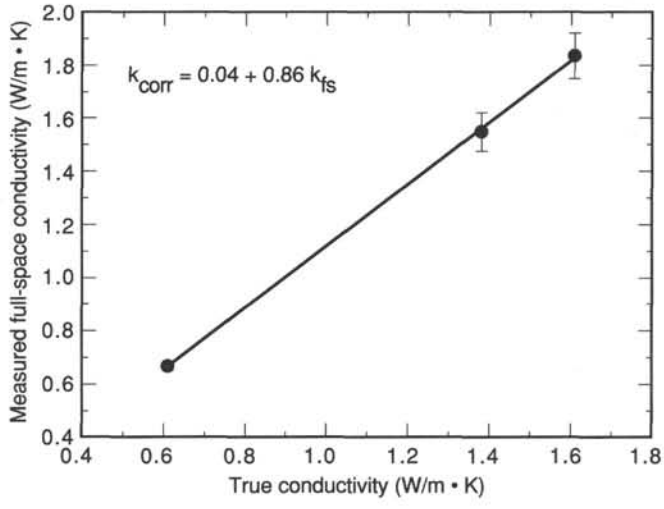

Figure 16. Measured and known thermal conductivities of full-space standards used during Leg 131. All data are listed in Table 8. Measured values are means and error bars showing one standard deviation. The line is a least-squares best fit, defined by the equation shown, used to correct all full-space measurements.

Table 10. Measured and known thermal conductivities of half-space standards.

Standard	Known conductivity	Probe 1[1]		Probe 4[1]		Probe 9[1]	
Fused silica	1.38	0.690	0.028 (8)	0.632	0.035(16)	0.666	0.024 (6)
Macor ceramic	1.61	0.827	0.014 (9)	0.722	0.038(10)	0.781	0.016(15)
basalt	1.93[2]	1.023	0.023(11)	0.912	0.072(11)	0.985	0.044 (5)

[1] Data for each probe include mean, standard deviation, and number of measurements.
[2] Thermal conductivity determined by the divided bar method at the U.S. Geological Survey, Menlo Park, CA Tectonophysics Branch, though subsequently revised (see text).

during the cruise and for this report. This difference may result in slightly different thermal conductivities, particularly for the higher thermally conductive sediments. No corrections have been made to the values of thermal conductivity reported in this volume that take into account the new calibration constants. However, preliminary review of the data correction shows most changes to thermal conductivity values are within the reported error.

Test Sequence

Several departures from standard ODP core-flow were followed during Leg 131 to provide a more comprehensive data base. Generally, whole-round samples were identified on the catwalk, but not cut until the section had been scanned in the MST. At Holes 808A and 808B, sections identified for whole-round sampling for chemical analyses (organic and inorganic) were run through the MST immediately and whole-rounds for consolidation/strength/structural studies were cut only after scanning. This approach was discontinued for Hole 808C, in which only magnetic susceptibility scans were collected after whole-round samples had been cut.

DOWNHOLE MEASUREMENTS

Scientific Objectives

Logging and downhole measurements were planned as a particularly large component of the Leg 131 program. Accurate and complete definitions of the structure, physical properties, and state of drilled sections are essential for the understanding of the deformation and dewatering processes involved in the development of accretionary wedges. In addition to a complete suite of standard logging tools, there are a number of special measurements designed to define the detailed structure, the geotechnical properties, temperature, and *in-situ* fluid compositions. The downhole measurements were directed in part to support the core analysis and other programs, and in part to obtain data that can be obtained only through downhole measurements.

Four log products were of particular importance for meeting the Leg 131 objectives:

Support of Detailed Structural Analysis of the Core

Logs provide continuous information on the physical stratigraphy, faults, fractures, and the features that are described in the core, allowing core data to be interpolated over low recovery and disturbed core sections. Of particular importance is the Lithoporosity tool string that obtains information on density and porosity, and the Formation Microscanner that provides a detailed conductivity image and thus a structural map of the borehole wall. Due to outside hole conditions it was not possible to deploy the FMS at all on Leg 131. Undisturbed cored intervals provided laboratory physical properties calibration for some of the logs.

Sediment Provenance and Alteration

The geochemical tool string can provide important information on sediment type and, in some cases, provenance. Turbidite sand-shale sections may be well delineated with this string. Channeled fluid flow, for example along thrusts, may be detected through alteration products. Hydrate could also be detected, both directly through the physical properties and through associated salinity changes.

Physical Properties

The standard downhole logs provide information on a wide range of *in-situ* physical properties at scales of tens of centimeters to tens of meters. These include seismic velocity, electrical resistivity, density, and porosity. A number of other characteristics may be qualitatively inferred, such as permeability, pore pressure, and thermal and geotechnical properties.

Correlation with Site Survey Data

The downhole logs provide direct correlation of in-hole structure with the seismic stratigraphy and velocity information from multichannel and other field seismic surveys, and with surface heat flow and other geophysical data. Thus the borehole may be put in the regional context provided by the site survey data. Synthetic seismograms may be computed using the combination of velocity and density logs.

Logging Operations

After coring is completed, downhole logs are completed either through the bit in the case of advance piston or extended core barrel coring, or after dropping the drill bit, in

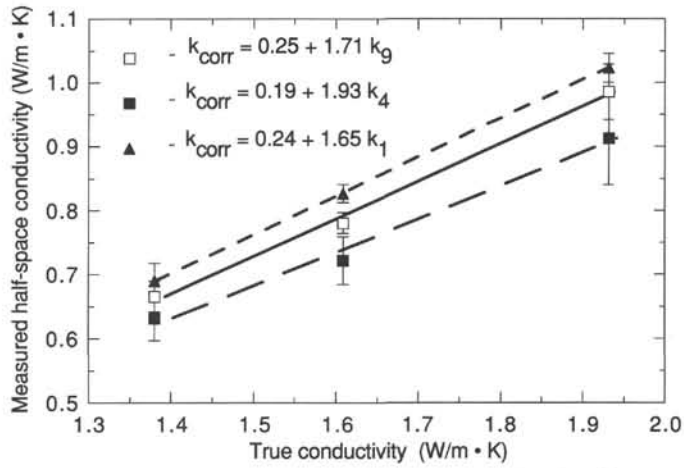

Figure 17. Measured and known thermal conductivities of half-space standards used during Leg 131. All data are listed in Table 9. Measured values are means and error bars showing one standard deviation. The lines are least-squares best fits, defined by the equations shown, used to correct all half-space measurements.

the case of rotary coring. Logging can also be completed after reentry without a drillbit. Each logging run consists of a combination of sensors lowered on a seven-conductor cable, with continuous monitoring in the logging laboratory. Tool depths are measured at the surface by the amount of wire run out. Because variable wire stretch leads to a depth error of up to several meters depth, cross-correlation between logs is provided by having a natural gamma tool on each lowering. Under rough sea conditions, a wireline heave-compensator is employed to minimize the effects of ship heave on the tool position in the borehole. A sidewall entry sub that allows the logging cable to enter the pipe beneath the ship may also be used to allow the drill pipe to be raised just ahead of the logging tools, thus maintaining a clear hole for the logs.

It is important to recognize the limitations of each of the tools, as discussed in the next section, to understand what each tool actually measures, what situations result in degraded data (notably washed out, large-diameter holes). The data are typically recorded at 15–24 cm (0.5-ft) depth intervals. The depths of investigation are sensor-dependent and range from only the borehole wall to several meters depth; common penetration is a few tens of centimeters. Some parameters such as resistivity are measured with several different depths of investigation; generally deeper penetration is traded against poorer vertical resolution. Four different tool strings of Schlumberger sensors were used on Leg 131, as outlined below.

Tool Strings

The three standard tool string configurations are shown in Figure 18. The long-spacing sonic configuration is shown in Figure 19.

Tool String No. 1–Seismic Stratigraphy (SDT/NGT/MCD/DIT)

a. Long-spacing digital sonic tool (SDT)–seismic stratigraphy and seismic velocity

b. Natural gamma spectrometry tool (NGT)–U, Th, K, and depth reference

c. Dual induction tool (DIT)–electrical conductivity and resistivity

d. Mechanical caliper device (MCD)–hole diameter and condition

e. High-resolution temperature tool (TLT)–Lamont temperature recorder.

Tool String No. 2–Lithoporosity (HLDT/CNT/NGT)

a. Lithodensity tool (HLDT)–formation density and lithology

b. Compensated neutron tool (CNT-G)–formation porosity

c. Natural gamma spectrometry tool (NGT)–U, Th, K, and depth reference

d. High-resolution temperature tool (TLT)–Lamont temperature recorder.

Tool String No. 3–Geochemical (GST/ACT/NGT)

a. Induced gamma spectroscopy tool (GST)–relative concentrations of a number of elements

b. Aluminum clay tool (ACT)–aluminum abundance

c. Natural gamma spectrometry tool (NGT)–U, Th, K, and depth reference

d. High-resolution temperature tool (TLT)–Lamont temperature recorder.

The Lamont-Doherty temperature tool (TLT) was attached at the base of each tool string to obtain high-resolution temperatures for thermal gradient determinations. A low-accuracy and relatively slow response-time Schlumberger continuous temperature log may be included in some of the tool strings.

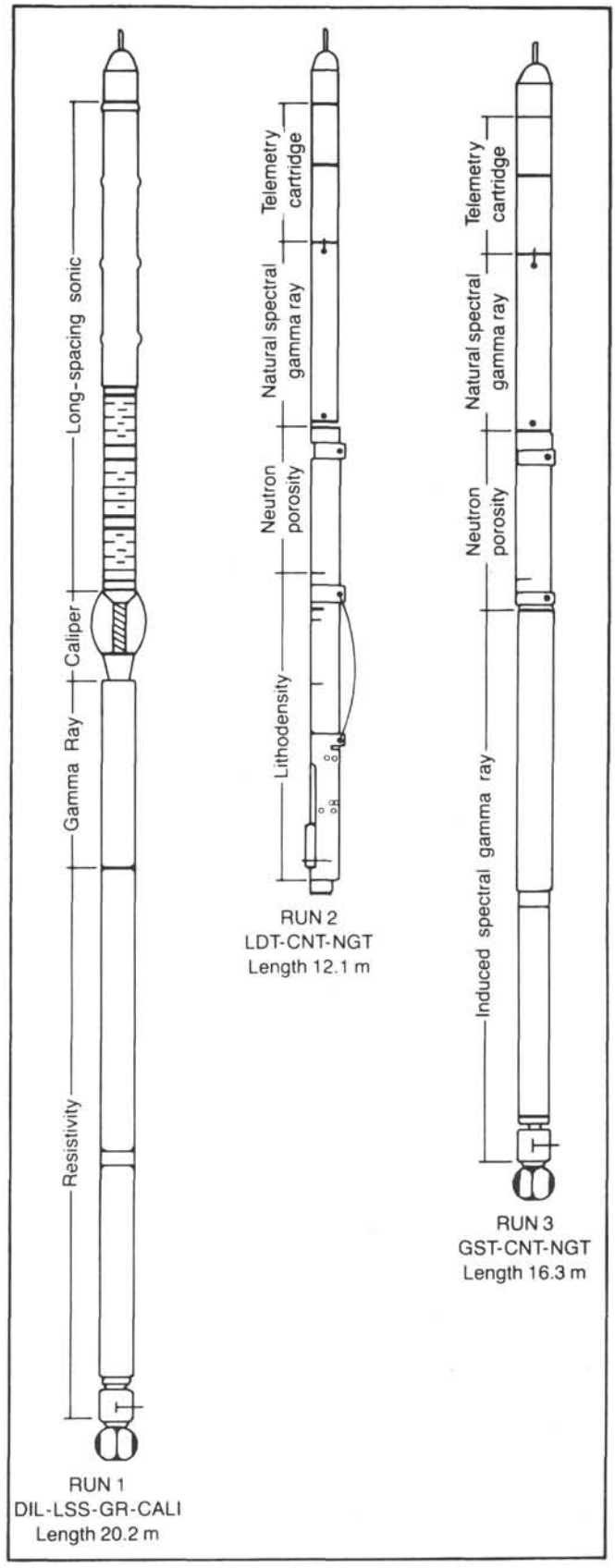

Figure 18. Schematic diagram showing the the tool configurations for the three standard tool strings run on Leg 131. The FMS tool string and the TLT temperature tool attached to the bottom of the first and third strings are not shown (from ODP Leg 107 Explanatory Notes, Fig. 13).

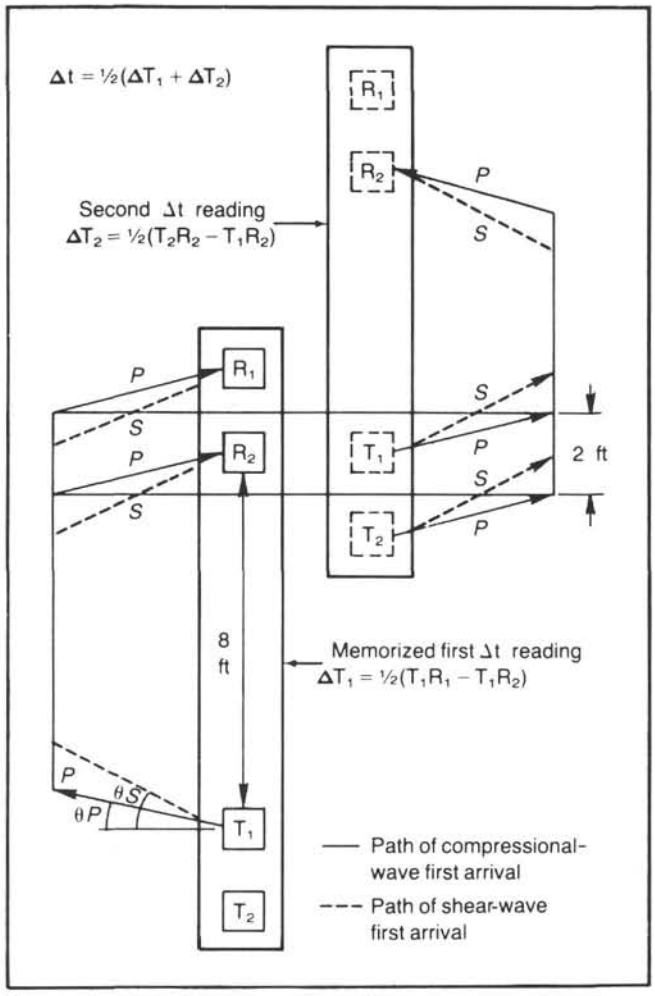

Figure 19. A schematic of the long-spacing sonic (LSS) velocity determination. The first time difference using the upward sound pulse travel is averaged with a second reading a fixed distance up the hole covering the same depth interval, using the downward sound pulse travel (from ODP Leg 107 Explanatory Notes, Fig. 15).

Device Descriptions

Aluminum Clay Tool (ACT)

Aluminum abundance is measured by the aluminum clay tool using a form of neutron activation analysis. A 2.5-MeV 252Cf source emits neutrons that are absorbed by aluminum, forming an unstable nucleus with a half-life of about 2 min. The decay of the nucleus emits characteristic gamma rays detected within a series of energy windows by the natural gamma tool. The contribution to the gamma-ray spectrum due to natural radiation is removed by running NGT tools both above and below the neutron source; the detector above measures the natural radiation before activation, and the detector below measures the induced plus natural radiation.

Compensated Neutron Porosity Tool (CNT)

Neutrons (5 MeV) emitted from an Am-Be source in the compensated neutron porosity tool lose energy primarily through collision with hydrogen in the formation. These slowed neutrons are then captured by elements such as Cl, Li, B, and Gd, and capture gamma rays are emitted. Thus the hydrogen content (occurring mainly in both bound and free water) of the formation is measured, expressed as thermal neutron porosity. The device also detects epithermal (intermediate energy) neutron flux, which is an indicator of free water only, expressed as epithermal neutron porosity. The difference between thermal neutron porosity and epithermal neutron porosity is thus proportional to bound water (in clays, etc.) within the formation. The thermal neutron capture cross-section from this log is also used with the neutron porosity in processing the geochemical logs. The vertical resolution of this tool is about 0.25 m.

Digital Sonic Tool (SDT)

The digital sonic tool uses two acoustic transmitters and two receivers to measure the time required for sound waves to travel through the borehole wall over source-receiver distances of 2.4, 3.0, and 3.6 m, i.e., an in-hole small-scale seismic refraction experiment. First arrivals for the individual source-receiver paths are used to calculate the velocities of the waves traveling in the formation; the tool measures four sonic velocities at each measurement depth as there are four possible paths. Only first-arrival compressional waves are determined aboard the ship, but the full sonic waveforms are recorded for post-cruise processing to allow semblance analysis of compressional velocities and determination of shear-wave and Stonely-wave velocities. The vertical resolution of the tool is about 0.61 m (2 ft). Logs can be corrected for cycle skipping (erroneous determination of the first- arrival wave) using the four-way measurement redundancy. Compressional-wave velocity is dominantly controlled by porosity; decreases in porosity with increasing consolidation and lithification typically cause velocity to increase with depth in a sedimentary sequence. The pore geometries, grain contacts, and grain compositions are important factors in the porosity-velocity relation.

The sonic tool can also provide a rough log of borehole diameter for use where a caliper log is not available.

Dual Induction Tool (DIT)

The dual induction tool provides three different measurements of electrical resistivity, each with a different radial depth of investigation. Two induction devices ("deep" and "medium" conductivity) send high-frequency alternating currents through transmitter coils, creating magnetic fields that induce secondary (Foucault) currents in the formation. These ground-loop currents produce new inductive signals, proportional to the conductivity of the formation, that are recorded by a series of receiving coils. A third device (the "spherically focused" resistivity, SFR) measures the current necessary to maintain a constant voltage drop across a fixed interval; it has a shallow depth of investigation. The vertical resolution is of the order of 2 m for the two induction devices and about 1 m for the SFR; the latter is of comparable resolution to that of the velocity tool. The data are corrected for irregularities in borehole diameter.

As a first approximation for most formations, resistivity is proportional to the pore fluid resistivity and roughly to the inverse square root of porosity (Archie's Law). The Humble formula commonly used in the petroleum industry has somewhat different coefficient and proportionality constants. The resistivity-porosity relation, normalized to the pore-fluid resistivity (formation factor), can be estimated from laboratory measurements on core. Borehole and formation fluid salinity and temperature, the geometry of the pore spaces, clay content, hydrocarbon content, hydrous and metallic minerals, and temperature all provide secondary control on electrical conductivity.

Gamma Spectroscopy Tool (GST)

The induced gamma spectroscopy tool consists of a pulsed 14-MeV neutron generator and a gamma-ray scintillation detector. The incident neutrons lose energy through inelastic scattering in the formation and eventually are captured by nuclei when they reach thermal energy levels (about 0.02 eV). After capture, gamma rays are emitted that are detected by the tool. The 256-channel energy spectrum is deconvolved to determine the relative abundance of Ca, Si, Fe, Cl, H, and S on board the ship. The raw logs are reprocessed by the Borehole Research Group at Lamont-Doherty Geological Observatory to obtain percentages of these elements and Gd and Ti. Because the depth of investigation is relatively shallow, the logs must also be corrected for variations in borehole diameter.

Lithodensity Tool (LDT)

The lithodensity tool uses a 0.66-MeV 137Ce gamma-ray source and a pair of detectors that are held against the hole wall with a pair of excentralizing bowsprings. The detectors measure the flux of transmitted gamma rays in a series of energy windows. The density estimate is based upon Compton scattering of the gamma rays within the formation, and thus actually is a measurement of electron density. As most rock-forming elements have atomic weights that are close to twice their atomic numbers, the electron density can be converted accurately to bulk density (a few elements do cause serious biases). The tool also records a photoelectric effect index. Photoelectric absorption occurs in the energy window below about 150 KeV. The measurement is almost independent of porosity and can therefore be used directly as a matrix lithology indicator. The density and photoelectric effect measurements require good contact with the borehole wall; the tool however, provides a measure of contact, and corrections can be made for excessive borehole roughness. The vertical resolution of the measurement is about 0.3 m.

Mechanical Caliper Device (MCD)

This tool provides a basic two-dimensional caliper log of the borehole by means of a three-arm bowspring-mounted measurement system. The hole diameter (HD) log is used to detect washouts or constrictions due to clay swelling. The caliper has a maximum extension of 40.6 cm (16 in.), so large diameter washouts are not measured accurately. Borehole diameter significantly affects many of the other logging measurements, and the hole diameter is an important input to log correction routines. It is also a vital factor in assessing tool safety during logging.

Natural Gamma Tool (NGT)

The natural (spectral) gamma tool measures the natural radioactivity of the formation in a series of energy windows. Most natural gamma rays are emitted by the naturally occurring radioactive isotope 40K and by a series of U and Th isotopes and their daughters. The gamma radiation from the formation close to the borehole wall is measured by a sodium iodide scintillation detector mounted inside the sonde. The energy spectrum is recorded from five discrete energy windows, which allows determination of the abundances of K, U, and Th. The data are corrected for borehole diameter variations. The tool has a depth of investigation of about 0.3–0.5 m. The tool is run on every combination tool string to provide depth correlations between runs.

K, U, and Th tend to be concentrated in clay minerals, consequently the gamma curve is used to provide a qualitative estimate of the sediment clay content. Uranium also tends to be concentrated in organic-rich sediments because of its redox chemistry and can be an indirect indicator of sapropelic layers. However, silicic volcaniclastics and K-feldspar-rich sandstones also can have high abundances of these three elements.

Lamont Temperature Tool (TLT)

The Lamont temperature tool is a self-contained high-precision logging tool with internal recording that is attached to the bottom of the Schlumberger tools (except the FMS) or the borehole televiewer. This tool provides much higher resolution, accuracy, and response than the Schlumberger temperature recorder that is included on some runs. There are two temperature sensors, a fast-response low-accuracy thermistor (CRCN8) that is designed to detect sudden very small temperature excursions caused by fluid flow into the borehole, and a slower response high-accuracy thermistor (YYSI9) that is intended for use in estimating the temperature gradient and thus heat flow. A high-precision pressure sensor provides depth control. Data from the two thermistors and the pressure transducer are collected and stored internally at a constant time interval selected in the range 0.5 to 5.0 s. The recording may be set to start at a preset pressure (depth).

As the data are recorded as a function of time, conversion to depth is based on the pressure-transducer, or on simultaneous recording of depth and time by other logs in the drill string. The conversion of pressure to depth requires knowledge of the density of the fluid in the pipe, i.e., seawater or drilling mud. Although the density of drilling mud put down the pipe prior to logging can be determined, the actual concentration after mixing with borehole fluids is unknown. Thus, the seafloor that is usually marked by a temperature discontinuity and the total depth must be used to provide pressure-to-depth calibration. A constant logging speed facilitates interpolation between these two points.

Tool Specifications

Maximum pressure range

To 69 MPa (10,000 psi); resolution: 69 KPa (10 psi).

Fast-response temperature sensor

Sampling rate 0.5 s, resolution 0.1 °C, range −40° to +150°C.

Slow-response temperature sensor

Sampling rate 2.5 s, resolution 0.01 °C. Range −40° to 150 °C. Temperatures above 110 °C require special high-temperature O-ring components.

Temperature and pressure data are recorded in the instrument data logging computer (ONSET Tattletale) at set time intervals until the tool is retrieved at the surface, or until the Tattletale memory limit of approximately 9 hr is reached. To read the data, one must open the tool and connect it to the Masscomp computer in the Downhole Measurements Laboratory. The data are loaded to a file for processing and merging with the time-depth record. Temperatures can then be displayed vs. depth. The time necessary for data recovery is approximately 30% of acquisition time.

Temperature Correction for Borehole Circulation

The borehole temperature record obtained is generally strongly disturbed by drilling fluid circulation. Thus, accurate estimates of formation temperatures require careful extrapolation of the measured drilling disturbed temperatures to equilibrium using drilling circulation records. This is facili-

tated by the continuous record of the rig floor operations that include: date, time, hook load (load of drill string), pump pressure, and pumping rate for each pump. Baseline offsets on the pumping-rate records need to be noted.

One stroke per minute (spm) equals 0.31 L/s. Each stroke of a three-cylinder pump is approximately 18.6 L; a common pumping rate of 60 spm with one pump operating is then 18.6 L/s. For example, a standard injection of logging mud is 60 spm x 54 min = 60,100 L, which corresponds to 378.0 barrels.

A number of approximate theories have been used to correct the measured borehole temperatures for circulation disturbance (see summary in Hyndman et al., 1977). One good method appears to be that of Jaeger (1961). If the fluid circulation rate is greater than about 25 L/s (80 spm) as is commonly the case for basalt basement holes, the hole can be assumed to be held at constant temperature equal to that of the bottom water during circulation. If the circulation rate is less than about 25 L/s as is commonly the case for sediment holes, the temperatures in the deeper parts of the hole during circulation can be significantly higher than bottom water temperatures (e.g., example of Burch and Langseth, 1981). In this case, the temperature disturbance must be estimated using the detailed record of circulation rate. In either case, the rate of recovery to equilibrium formation temperatures is dependent on the duration of the disturbance and the time since the disturbance ended. Having two or more temperature logs at different times greatly facilitates accurate estimation of formation temperatures.

Vertical Seismic Profile–Well Seismic Tool (WST)

A vertical seismic profile (VSP) experiment was included in Leg 131 to determine the detailed velocity-depth structure of the drilled section and to provide an accurate correlation between the drilled section and the site survey seismic reflection data. VSP measurements provide such seismic information for the interfaces penetrated by the borehole, and they also allow delineation of reflecting interfaces below the bottom of the borehole (Gal'perin 1974).

The seismic source for the VSP is a single 6.6-L (400-in.3) water gun suspended from a buoy at about 10 m water depth. The signals are received by the standard Schlumberger Well Seismic Tool (WST) clamped at depth intervals in the hole and recorded with the Schlumberger logging computer. The depth interval used for the VSP during Leg 131 was 12.2 m (40 ft). Several shots were fired at each level within the borehole to allow stacking of the data. Initial on-board processing was accomplished with the Schlumberger Quick-Look software.

Water Sampler, Temperature, Pore-Pressure Tool (WSTP)

This tool has a thin, stainless-steel probe that is pushed ahead of the bit into the undisturbed sediments at the bottom of the hole (Fig. 20). The instrument can measure either sediment temperature or pore-fluid pressure, and it can collect a pore-water sample at a pre-set time. When configured to measure temperature, the tool consists of a thermistor mounted at the end of the probe, a self-contained recorder, a timer to open the fluid-sampling valve, and a 16-V power supply. In pore-pressure configuration, the instrument is fitted with a hollow probe tipped with a sintered stone, allowing a hydraulic connection between the end of the probe and an absolute pressure transducer. A second transducer is configured to monitor hydrostatic pressure. Pore fluid is collected through a filter block above the probe (Barnes, 1988).

In operation, the WSTP is mounted inside a core barrel and lowered down the drill pipe by wireline while the bit is held above the bottom of the hole. The tool is held briefly above

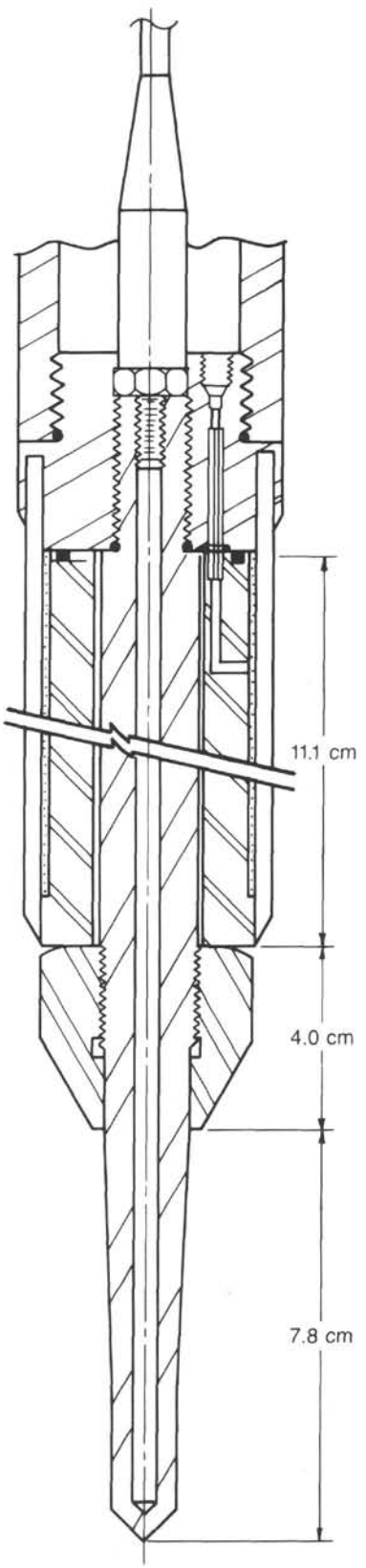

Figure 20. Cross section of the WSTP tool thermistor probe/pore-pressure probe assembly. The diameter of the probe is about 1.3 cm, the diameter of the filter block behind the probe has a diameter of 5.0 cm, and the main shaft of the tool has a diameter of 6.0 cm (from ODP Leg 117 Explanatory Notes, Fig. 10).

mudline to measure reference values of either temperature or pressure. The tool is then lowered and latched into place with the probe tip extending 1.1 m ahead of the bit. The drill string is lowered and the probe is forced into the bottom. A collated delivery system allows the probe to retract back up inside the bit, should the formation prove to be too hard for penetration. With an APC/XCB bottom hole assembly, the bit can be decoupled from the tool after penetration so that the probe will not be disturbed by drill string heave.

Penetration of about 70 cm is required within about 3 hr of drilling for the temperature of the formation to be undisturbed by the effects of cold circulation fluid. The thermistor/recording package has a nominal resolution of about 10 ohms, or 0.01°C at 25°C. The relatively short length of the narrow probe appears to allow only a few minutes of undisturbed measurements before a thermal disturbance is conducted down from the larger-diameter section above, limiting the accuracy of temperature extrapolations to about ±0.1°–0.2°C. The pressure transducers have a resolution of about 8–10 psi.

There is significant disturbance of the formation resulting from insertion of the probe, but as the instrument cannot be left in position to allow this disturbance to decay completely, extrapolation to equilibrium is required. The thermal response of a cylindrical probe to a pulse of heating (or cooling) is given by the F(alpha,tau) function described by Bullard (1954). This function approaches 1/t after several minutes, given the small diameter of the probe. The 1.27-cm diameter probe has a thermal time constant of about 2–3 min, depending on the thermal diffusivity of the sediments, requiring that the probe be kept in bottom for at least 5–10 min. The theoretical decay curves assume an instantaneous heating of the probe on penetration, although a finite time is required for the thermistor to reach its maximum temperature. As a result, the effective origin time of the pulse is delayed as a function of probe and sediment properties. In addition, the recording packages sample temperatures at intervals of 5–60 s, leaving the exact penetration time uncertain. An effective penetration time is estimated by matching the decay of the thermal pulse to the theoretical curve. The theory of measurement was given in Erickson et al. (1975). A review of thermal data obtained with this type of probe during the DSDP is given in Hyndman et al. (1987).

Special Downhole Tools

A number of special downhole tools and experiments were included in Leg 131 in addition to the suite of logs and other downhole tools described above. They are outlined below but described in detail in the special tools chapter, this volume.

Borehole Packers

Packers are used to obtain downhole permeability and pore pressure, and to sample fluid from the formation. The drill string packer was used on Leg 131.

Lateral Stress Tool (LAST)

The Lateral Stress Tool measures *in-situ* lateral stress components at the bottom of the hole, along with effective pore pressure and temperature.

Long-Term Temperature Recording System (ONDO)

The ONDO system includes a string of temperature sensors and a recording package that allows the recording of downhole temperature for several years after the drill ship has departed. The recorded data can be recovered periodically by an oceanographic ship through an acoustic interrogation system.

REFERENCES

ASTM, 1989. Annual Book of ASTM Standards for Soil and Rock, Building Stones: *Geotextiles*. 0408: Philadelphia (Am. Soc. for Testing and Materials).

Backman, J., and Pestiaux, P., 1986. Pliocene *Discoaster* abundance variations, Deep Sea Drilling Project Site 606: biochronology and paleoenvironmental implications. *In* Ruddiman, W. F., Kidd, R. B., Thomas, E., et al., *Init. Repts. DSDP*, 94 (Pt. 2): Washington (U.S. Govt. Printing Office), 903–910.

Backman, J., Schneider, D. A., Rio, D., and Okada, H., 1990. Neogene low-latitude magnetostratigraphy from Site 710 and revised age estimates of Miocene nannofossil datum events. *In* Duncan, R. A., Backman, J., Peterson, L. C., et al., *Proc. ODP, Sci. Results*, 115: College Station, TX (Ocean Drilling Program), 271–276.

Backman, J., and Shackleton, N. J., 1983. Quantitative biochronology of Pliocene and early Pleistocene calcareous nannofossils from the Atlantic, Indian and Pacific oceans. *Mar. Micropaleontol.*, 8:141–170.

Barnes, R. O., 1988. ODP *in situ* fluid sampling and measurement: a new wireline tool. *In* Mascle, A., Moore, J. C., et al., *Proc. ODP, Init. Repts.*, 110: College Station, TX (Ocean Drilling Program), 55–63.

Berggren, W. A., Kent, D. V., and Flynn, J. J., 1985. Jurassic to Paleogene: Part 2. Paleogene geochronology and chronostratigraphy. *In* Snelling, N. J. (Ed.), *The Chronology of the Geological Record*. Geol. Soc. London Mem., 10:141–195.

Berggren, W. A., Kent, D. V., Flynn, J. J., and Van Couvering, J. A., 1985. Cenozoic geochronology. *Geol. Soc. Am. Bull.*, 96:1407–1418.

Berggren, W. A., Kent, D. V., and Van Couvering, J. A., 1985. The Neogene: Part 2. Neogene geochronology and chronostratigraphy. *In* Snelling, N. J. (Ed.), *The Chronology of the Geological Record*. Geol. Soc. London Mem., 10:211–260.

Blatt, H., Middleton, G. V., and Murray, R., 1980. *Origin of Sedimentary Rocks* (2nd ed.): Englewood Cliffs, NJ (Prentice-Hall).

Boyce, R. E., 1976. Definitions and laboratory techniques of compressional sound velocity parameters and wet-water content, wet-bulk density, and porosity parameters by gravimetric and gamma ray attenuation techniques. *In* Schlanger, S. O., Jackson, E. D., et al., *Init. Repts. DSDP*, 33: Washington (U.S. Govt. Printing Office), 931–958.

Bullard, E. C., 1954. The flow of heat through the floor of the Atlantic Ocean. *Proc. R. Astron. Soc. London*, A222:408–429.

Burch, J. K., and Langseth, M. G., 1981. Heat-flow determination in three DSDP boreholes near the Japan Trench. *J. Geophys. Res.*, 86:9411–9419.

Clark, S. P., (Ed.), 1966. *Handbook of Physical Constants:* Mem. Geol. Soc. Am., 97.

Cook, H. E., Johnson, P. D., Matti, J. C., and Zemmels, I., 1975. Methods of sample preparation and X-ray diffraction data analysis, X-ray Mineralogy Laboratory, Deep Sea Drilling Project, University of California, Riverside. *In* Hayes, D. E., and Frakes, L. A., et al., *Init. Repts. DSDP*, 28: Washington (U.S. Govt. Printing Office), 999–1007.

Donnelly, T. W., 1980. Appendix. Chemical composition of deep sea sediments - Sites 9 through 425, Legs 2 through 54, DSDP. *In* Rosendahl, B. R., Hekinian, R., et al., *Init. Repts. DSDP*, 54: Washington (U.S. Govt. Printing Office), 899–949.

Dunham, R., 1962. Classification of carbonate rocks according to depositional texture. *In* Ham, W. E. (Ed.), *Classification of Carbonate Rocks:* Tulsa (AAPG), 108–121.

Emeis, K.-C., and Kvenvolden, K. A., 1986. Shipboard organic geochemistry on *JOIDES Resolution*. *ODP Tech. Note*, 7.

Erickson, A. J., Von Herzen, R. P., Sclater, J. P., Girdler, R. W., Marshall, B. V., and Hyndman, R. D., 1975. Geothermal measurements in deep-sea boreholes. *J. Geophys. Res.*, 80:2515–2528.

Espitalié, J., Deroo, G., and Marquis, F., 1985a. La pyrolyse Rock-Eval et ses applications. *Rev. Inst. Fr. Pet.*, 40:563–579.

_____, 1985b. La pyrolyse Rock-Eval et ses applications. *Rev. Inst. Fr. Pet.*, 40:755–784.
_____, 1986. La pyrolyse Rock-Eval et ses applications. *Rev. Inst. Fr. Pet.*, 41:73–89.
Fisher, R. V., and Schmincke, H.-U., 1984. *Pyroclastic Rocks:* New York (Springer-Verlag).
Fornaciari, E., Raffi, I., Rio, D., Villa, G., Backman, J., and Olafsson, G., 1990. Quantitative distribution patterns of Oligocene and Miocene calcareous nannofossils from the western equatorial Indian Ocean. *In* Backman, J., Duncan, R. A., et al., *Proc. ODP, Sci. Results,* 115: College Station, TX (Ocean Drilling Program), 237–254.
Franzini, M., Leoni, L., and Saitta, M., 1975. Revisione di una metodologia analitica per fluorescenza-X, basata sulla correzione completa degli effetti di matrice. *Rend. Soc. Ital. Mineral. Petrol.*, 31:365–378.
Gal'perin, E. I., 1974. *Vertical Seismic Profiling:* Soc. Explor. Geophys. Spec. Publ., 12.
Gieskes, J. M., 1973. Interstitial water studies, Leg 15: alkalinity, pH, Mg, Ca, Si, PO4, and NH_4. *In* Heezen, B. C., MacGregor, I. D., et al., *Init. Repts. DSDP,* 20: Washington (U.S. Govt. Printing Office), 813–829.
_____, 1974. Interstitial water studies, Leg 25. *In* Simpson, E.S.W., Schlich, R., et al., *Init. Repts. DSDP,* 25: Washington (U.S. Govt. Printing Office), 361–394.
Gieskes, J. M., and Gamo, T., in press. Wet chemical analysis of sediments for major element composition. *ODP Tech. Note.*
Gieskes, J. M., Gamo, T., and Brumsack, H. J., in press. Chemical methods for interstitial water analysis on *JOIDES Resolution. ODP Tech. Note.*
Gieskes, J. M., and Peretsman, G., 1985. Water chemistry procedures aboard *JOIDES Resolution* - some comments. *ODP Tech. Note, 5.*
Hamilton, E. L., 1971. Prediction of *in-situ* acoustic and elastic properties of marine sediments. *Geophysics,* 36:266–284.
Hay, W. W., 1970. Calcareous nannofossils from cores recovered on DSDP Leg 4. *In* Bader, R. G., Gerard, R. D., et al., *Init. Repts. DSDP,* 4: Washington (U.S. Govt. Printing Office), 455–501.
Hyndman, R. D., Langseth, M. G., and Von Herzen, R. P., 1987. Deep Sea Drilling Project geothermal measurements: a review. *Rev. Geophys.,* 25:1563–1582.
Hyndman, R. D., Von Herzen, R. P., Erickson, A. J., and Jolivet, J., 1977. Heat-flow measurements, DSDP Leg 37. *In* Aumento, F., Melson, W. G., et al., *Init. Repts. DSDP,* 37: Washington (U.S. Govt. Printing Office), 347–362.
Jaeger, J. C., 1961. The effect of the drilling fluid on temperatures measured in boreholes. *J. Geophys. Res.,* 66:563–569.
Johnson, D. A., and Nigrini, C. A., 1985. Synchronous and time-transgressive Neogene radiolarian datum levels in the equatorial Indian and Pacific Oceans. *Mar. Micropaleontol.,* 9:489–523.
Lee, T.-C., 1989. Thermal conductivity measured with a line source between two dissimilar media equals their mean conductivity. *J. Geophys. Res.,* 94:12443–12447.
Leoni, L., and Saitta, M., 1976. X-ray flourescence analyses of 29 trace elements in rock and mineral standards. *Rend. Soc. Ital. Mineral. Petrol.,* 32:497–510.
Lundberg, N., and Moore, J. C., 1986. Macroscopic structural features in Deep Sea Drilling Project cores from forearc regions. *In* Moore, J. C. (Ed.), *Structural Fabrics Preserved in Deep Sea Drilling Project Cores From Forearcs:* Mem. Geol. Soc. Am., 166:13–44.
Martini, E., 1971. Standard Tertiary and Quaternary calcareous nannoplankton zonation. *In* Farinacci, A. (Ed.), *Proc. 2nd Planktonic Conf. Roma:* Rome (Ed. Technosci.), 2:739–785.
Mazzullo, J. M., Meyer, A., and Kidd, R., 1987. New sediment classification scheme for the Ocean Drilling Program. *In* Mazzullo, J., and Graham, A. G., *Handbook for Shipboard Sedimentologists.* ODP Tech. Note, 8:45–67.
Munsell Soil Color Charts, 1971. Baltimore (Munsell Color).
Nigrini, C., and Caulet, J.-P., 1988. The genus *Anthocyrtidium* (Radiolaria) from the tropical late Neogene of the Indian and Pacific Oceans. *Micropaleontology,* 34:341–360.
Pettijohn, E. J., Potter, P. E., and Siever, R., 1973. *Sand and Sandstone*: New York (Springer-Verlag).
Powell, P. W., 1958. Thermal conductivity and expansion coefficients of water and ice. *Adv. Phys.,* 10:22–25.
Pyle, M. R., 1984. Vane shear data on undrained residual strength. *J. Tech. Div. Am. Soc. Civ. Eng.,* 110:543–547.
Ratcliffe, E. H., 1959. Thermal conductivities of fused and crystalline quartz. *Br. J. Appl. Physics,* 7:276–297.
_____, 1960. The thermal conductivities of ocean sediments. *J. Geophys. Res.,* 65:1535–1541.
Riedel, W. R., and Sanfilippo, A., 1978. Stratigraphy and evolution of tropical Cenozoic radiolarians. *Micropaleontology,* 24:61–96.
Rio, D., Backman, J., and Raffi, I., 1988. *Calcareous Nannofossil Biochronology and the Pliocene/Pleistocene Boundary:* Cambridge (Cambridge Univ. Press).
Rio, D., Fornaciari, E., and Raffi, I., 1990. Late Oligocene through early Pleistocene calcareous nannofossils from western equatorial Indian Ocean (ODP Leg 115). *In* Duncan, R. A., Backman, J., Peterson, L. C., et al., *Proc. ODP Sci. Results.,* 115: College Station, TX (Ocean Drilling Program), 175–236.
Sanfilippo, A., Westberg-Smith, M. J., and Riedel, W. R., 1985. Cenozoic radiolaria. *In* Bolli, H. M., Saunders, J. B., and Perch-Nielsen, K. (Eds.), *Plankton Stratigraphy:* Cambridge (Cambridge Univ. Press), 631–712.
Sass, J. H., Kennelly, J. P., Jr., Smith, E. P., and Wendt, W. E., 1984. Laboratory line-source methods for the measurement of thermal conductivity of rocks near room temperature. *U.S. Geol. Surv. Tech. Rept.*
Sato, T., Kameo, K., and Takayama, T., in press. Coccolith biostratigraphy of the Arabian Sea and a new nannofossil zonal scheme for the Quaternary. *In* Prell, W. L., Niitsuma, N., et al., *Proc. ODP, Sci. Results,* 117: College Station, TX (Ocean Drilling Program).
Sayles, F. L., Manheim, F. T., and Waterman, L. S., 1973. Interstitial water studies on small core samples, Leg 15. *In* Heezen, B. C., MacGregor, I. D., et al., *Init. Repts. DSDP,* 20: Washington (U.S. Govt. Printing Office), 783–804.
Shepard, F. P., 1954. Nomenclature based on sand-silt-clay ratios. *J. Sediment. Petrol.,* 24:151–158.
Shipboard Scientific Party, 1989. Explanatory notes. *In* Prell, W. L., Niitsuma, N., et al., *Proc. ODP, Init. Repts.,* 117: College Station, TX (Ocean Drilling Program), 11–34.
_____, 1990a. Explanatory notes. *In* Rangin, C., Silver, E. A., et al., *Proc. ODP, Init. Repts.,* 124: College Station, TX (Ocean Drilling Program), 7–33.
_____, in press. Introduction and explanatory notes. *In* Larson, R., and Lancelot, Y., et al., *Proc. ODP, Init. Repts.,* 129: College Station, TX (Ocean Drilling Program).
_____, 1990b. Introduction and explanatory notes. *In* Pisciotto, K., and Tamaki, K., et al., *Proc. ODP, Init. Repts.,* 127: College Station, TX (Ocean Drilling Program), 35–59.
Thierstein, H. R., Geitzenauer, K. R., Molfino, B., and Shackleton, N. J., 1977. Global synchroneity of late Quaternary coccolith datum levels: validation by oxygen isotopes. *Geology,* 5:400–404.
Vacquier, V., 1985. The measurement of thermal conductivity of solids with a transient linear heat source on the plane surface of a poorly conducting body. *Earth Planet. Sci. Lett.,* 74:275–279.
Von Herzen, R. P., and Maxwell, A. E., 1959. The measurement of thermal conductivity of deep-sea sediments by a needle probe method. *J. Geophys. Res.,* 65:1557–1563.
Zijderveld, J.D.A., Zachariasses, J. W., Verhallen, P.J.J.M., and Hilgen, F. J., 1986. The age of the Miocene-Pliocene boundary. *Newsl. Stratigr.,* 16:169–181.

Ms 131A-104